Article

NLRs guard metabolism to coordinate pattern- and effector-triggered immunity

https://doi.org/10.1038/s41586-021-04219-2

Received: 6 October 2020

Accepted: 9 November 2021

Published online: 15 December 2021

Check for updates

Keran Zhai[1,7], Di Liang[1,2,7], Helin Li[1,3], Fangyuan Jiao[1,4], Bingxiao Yan[1,2], Jing Liu[1,2], Ziyao Lei[1,2], Li Huang[1,2], Xiangyu Gong[1,2], Xin Wang[1], Jiashun Miao[1], Yichuan Wang[5], Ji-Yun Liu[1], Lin Zhang[6], Ertao Wang[1], Yiwen Deng[1], Chi-Kuang Wen[1], Hongwei Guo[5], Bin Han[1] & Zuhua He[1,4]✉

Pattern-triggered immunity (PTI) and effector-triggered immunity (ETI) in plants enable them to respond to pathogens by activating the production of defence metabolites that orchestrate immune responses[1–4]. How the production of defence metabolites is promoted by immune receptors and coordinated with broad-spectrum resistance remains elusive. Here we identify the deubiquitinase PICI1 as an immunity hub for PTI and ETI in rice (*Oryza sativa*). PICI1 deubiquitinates and stabilizes methionine synthetases to activate methionine-mediated immunity principally through biosynthesis of the phytohormone ethylene. PICI1 is targeted for degradation by blast fungal effectors, including AvrPi9, to dampen PTI. Nucleotide-binding domain, leucine-rich-repeat-containing receptors (NLRs) in the plant immune system, such as PigmR, protect PICI1 from effector-mediated degradation to reboot the methionine–ethylene cascade. Natural variation in the *PICI1* gene contributes to divergence in basal blast resistance between the rice subspecies *indica* and *japonica*. Thus, NLRs govern an arms race with effectors, using a competitive mode that hinges on a critical defence metabolic pathway to synchronize PTI with ETI and ensure broad-spectrum resistance.

Plants have evolved a two-tiered immune system that consists of PTI and ETI[1]. PTI is controlled by pattern recognition receptors (PRRs) on the plasma membrane that recognize pathogen-associated molecular patterns (PAMPs)[2]. Pathogens deliver effectors to attenuate plant PTI[3]. Plants then evolved intracellular NLR receptors to recognize pathogen effector perturbations and activate ETI[4], which have been widely adopted in crop breeding for disease resistance[5]. PTI and ETI have recently been proposed to be mutually potentiating[6,7], and they trigger similar biosynthesis of a diverse set of defence-related secondary metabolites and phytohormones[8]. Methionine (Met) is the precursor of ethylene[9], and pathogen effectors hijack the ethylene pathway to favour colonization[10,11]. Although primary metabolites have been proposed to be involved in plant defence, their immune function and the mechanisms by which NLRs guard and activate their biosynthesis are unclear. How NLRs dominate the arms race against pathogen effectors to orchestrate effective immune responses has long been a puzzle. *Magnaporthe oryzae* causes blast, the most destructive rice disease[12]. *M. oryzae* secretes effectors into the host cell[13–20]. Several NLRs that confers broad-spectrum blast resistance have been isolated[21–23], but how these NLRs act remains largely unknown.

PICI1 functions in ETI

The rice NLR PigmR confers resistance to all fungal blast races tested[21], suggesting that it potentially integrates PTI and ETI to ensure broad-spectrum resistance. To identify potential signalling regulators, we performed a combined analysis of PigmR-interacting proteins using a yeast-two hybrid (Y2H) screen (referred to as ETI-related proteins) and chitin-induced proteins by quantitative proteomics (referred to as PTI-related proteins), which yielded three overlapping candidates (Extended Data Fig. 1a, Supplementary Table 1). Among these PigmR-interacting and chitin-induced proteins (PICIs), PICI1 contains a PPPDE domain that is conserved in eukaryotes including humans[24], and which is predicted to be a new class of deubiquitinatase (Extended Data Fig. 1b). PigmR specifically interacted with PICI1 through its coiled-coil domain in the Y2H screen and in a split luciferase complementation (SLC) assay (Fig. 1a, Extended Data Fig. 1c–h). PICI1–GFP co-localized with PigmR (Extended Data Fig. 1i–l) and co-immunoprecipitated with PigmR–7Myc–6His (Fig. 1b). We generated transgenic plants in a wild-type near-isogenic *Pigm* line (NIL-*Pigm*)[21] (Extended Data Fig. 2a, b), and found that knockout of *PICI1* (*PICI1*-KO) significantly decreased resistance to avirulent TH12 compared to NIL-*Pigm* and *PICI1*-OE (*PICI1* overexpression) (Fig. 1c, Extended Data Fig. 2c). PICI1 also interacted with the coiled-coil domains of Pi9 and Pizt[23]—which confer similar blast resistance to *PigmR*[21]—but did not interact with Pish, which confers limited race resistance[21] (Extended Data Fig. 2d–h). *PICI1*-KO in *Pizt* and *Pi9* lines, but not in *Pish*, decreased resistance to avirulent strains (Extended Data Fig. 2i–q), suggesting that PICI1 is required for full ETI by directly interacting with specific NLRs. We next transiently expressed the blast effector AvrPizt in Pizt-containing rice cells[20], which is expected to activate only ETI in the absence of PAMPs. We observed that cell death mediated by the Pizt–AvrPizt interaction was decreased

[1]National Key Laboratory of Plant Molecular Genetics, CAS Center for Excellence in Molecular Plant Sciences, Institute of Plant Physiology and Ecology, Chinese Academy of Sciences, Shanghai, China. [2]University of the Chinese Academy of Sciences, Beijing, China. [3]School of Life Sciences, Henan University, Kaifeng, China. [4]School of Life Science and Technology, Shanghai Tech University, Shanghai, China. [5]Department of Biology, Institute of Plant and Food Science, Southern University of Science and Technology, Shenzhen, China. [6]Jiangsu Key Laboratory of Crop Genomics and Molecular Breeding, Yangzhou University, Yangzhou, China. [7]These authors contributed equally: Keran Zhai, Di Liang. ✉e-mail: zhhe@cemps.ac.cn

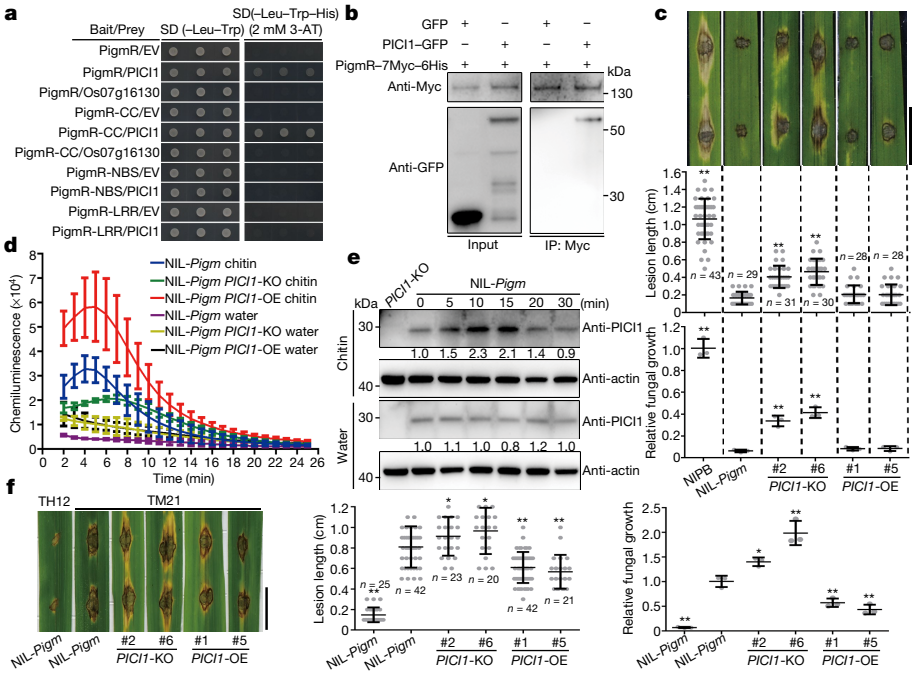

Fig. 1 | PICI1 interacts with PigmR and regulates PigmR-mediated blast resistance and PTI responses. a, PigmR interacts with PICI1 in a Y2H assay. EV, empty vector; SD (–Leu–Trp) and SD (–Leu–Trp–His), SD medium lacking essential amino acids; 3AT, 3-aminotriazole. Another chitin-induced protein Os07g16130 served as a negative control. **b**, Co-IP of PigmR–7Myc–6His and PICI1–GFP. GFP served as a negative control. **c**, NIL-*Pigm*, *PICI1*-KO and *PICI1*-OE/NIL-*Pigm* lines, 5 days post-inoculation (dpi) with punch inoculation (avirulent isolate TH12). NIPB served as a susceptible control. **d**, Chitin-induced ROS burst. Data are mean ± s.d. ($n = 9$, biologically independent samples). **e**, PICI1 was induced after chitin treatment. Leaf sheaths were collected at different times of chitin incubation, with water as a control. Relative PICI1 abundance is indicated with *PICI1*-KO as a negative control. **f**, Basal blast resistance of wild-type and transgenic lines of *PICI1*-KO and *PICI1*-OE in NIL-*Pigm*, 5 dpi with the virulent strain TM21. Avirulent TH12 served as a resistant control. For **c**, **f**, data were analysed by two-tailed Student's *t*-test. Fungal growth (mean ± s.d.; $n = 3$, biologically independent samples), lesion lengths (mean ± s.d.; n = number of biologically independent samples in the graph). Scale bars, 1 cm. Asterisks represent significant differences (*$P < 0.05$, **$P < 0.01$). Exact P values are provided in Supplementary Table 4. Similar results were obtained from three (**a**, **c**–**f**) or two (**b**) independent experiments.

in *PICI1*-KO (Extended Data Fig. 2r, s), which suggests that PICI1 has a bona fide role in NLR-mediated ETI. Together, these data show that PICI1 has a general role in ETI.

PICI1 functions in PTI

Next, we investigated the potential role of PICI1 in PTI. We found that the chitin-induced production of reactive oxygen species (ROS) and expression of pathogen-related genes were suppressed in *PICI1*-KO but enhanced in *PICI1*-OE (Fig. 1d, Extended Data Fig. 3a). Moreover, chitin induced the expression of *PICI1* mRNA and the accumulation of PICI1 protein (Fig. 1e, Extended Data Fig. 3b), similar to PTI triggered by TM21 (a TH12 mutant that is virulent to PigmR) (Extended Data Fig. 3c–e). Consistently, *PICI1*-KO enhanced susceptibility whereas *PICI1*-OE increased resistance to TM21 (Fig. 1f). Similar results were also observed with susceptible Nipponbare (NIPB) plants treated with chitin or *M. oryzae* (Extended Data Fig. 3f–i). The PRR OsCERK1 is essential for chitin signalling[25]. *PICI1*-OE/*OsCERK1*-KO decreased—whereas the *PICI1*-KO/*OsCERK1*-KO double mutant did not affect—susceptibility to TH12 compared to *OsCERK1*-KO (Extended Data Fig. 3j–n), suggesting that PICI1 acts downstream of OsCERK1-mediated PTI.

Furthermore, ROS production and pathogen-related gene expression induced by the bacterial elicitor flg22 were suppressed in *PICI1*-KO but enhanced in *PICI1*-OE (Extended Data Fig. 3o, p). PICI1 was also induced by flg22 and by infection with bacterial *Xanthomonas oryzae* pv. *oryzae* (*Xoo*) (Extended Data Fig. 3q, r). *PICI1*-KO enhanced susceptibility, but *PICI1*-OE increased resistance, to *Xoo* (Extended Data Fig. 3s). Thus, PICI1 has a critical role in rice PTI. Notably, *PICI1*-KO in NIPB (hereafter, *PICI1*-KO/NIPB) compromised PTI but not Pish-mediated ETI (Extended Data Figs. 2q, 3i), suggesting that PICI1-mediated PTI could be decoupled from ETI.

PICI1 is a plant deubiquitinase

We next determined that recombinant PICI1 and the PPPDE domain of PICI1 (PICI1-PPPDE) cleaved the ubiquitin-AMC substrate (Fig. 2a), towards K48- and K63-linked but not linear ubiquitin (Extended Data Fig. 4a), suggesting that PICI1 is a deubiquitinase. Cys115 in the catalytic dyad, a well-recognized residue in human isopeptide cleavage[26], is critical for the activity of PICI1 (Fig. 2a, Extended Data Fig. 4b). Moreover, chitin-induced expression of pathogen-related genes was compromised in protoplasts expressing PICI1(C115S), suggesting its essential role for immune activation (Extended Data Fig. 4c).

We next observed an increased abundance of ubiquitin-conjugated proteins—particularly K48-linked ubiquitin, which is critical for protein turnover[27]—in *PICI1*-KO compared with the wild type, which was further enhanced after treatment with chitin (Fig. 2b). The decreased resistance was associated with increased ubiquitination in *PICI1*-KO, which was abolished after infection with TM21 (Extended Data Fig. 4d). Thus, PICI1-mediated deubiquitination is likely to be involved in PigmR-mediated immunity. PICI1 is therefore a deubiquitinase that was previously unknown, to our knowledge, and which does not affect plant growth (Extended Data Fig. 4e).

PICI1 stabilizes methionine synthase

To identify direct substrates of PICI1, we performed PICI1–GFP immunoprecipitation followed by mass spectroscopy (IP–MS) and then intersected potential PICI1-associated proteins with the chitin-induced ubiquitome[28], which yielded 20 ubiquitin-modified candidates, including a Met synthase (LOC_Os12g42876) that is highly conserved in monocots and dicots (hereafter named OsMETS1) (Extended Data Fig. 4f–h, Supplementary Table 1). We confirmed the PICI1–OsMETS1

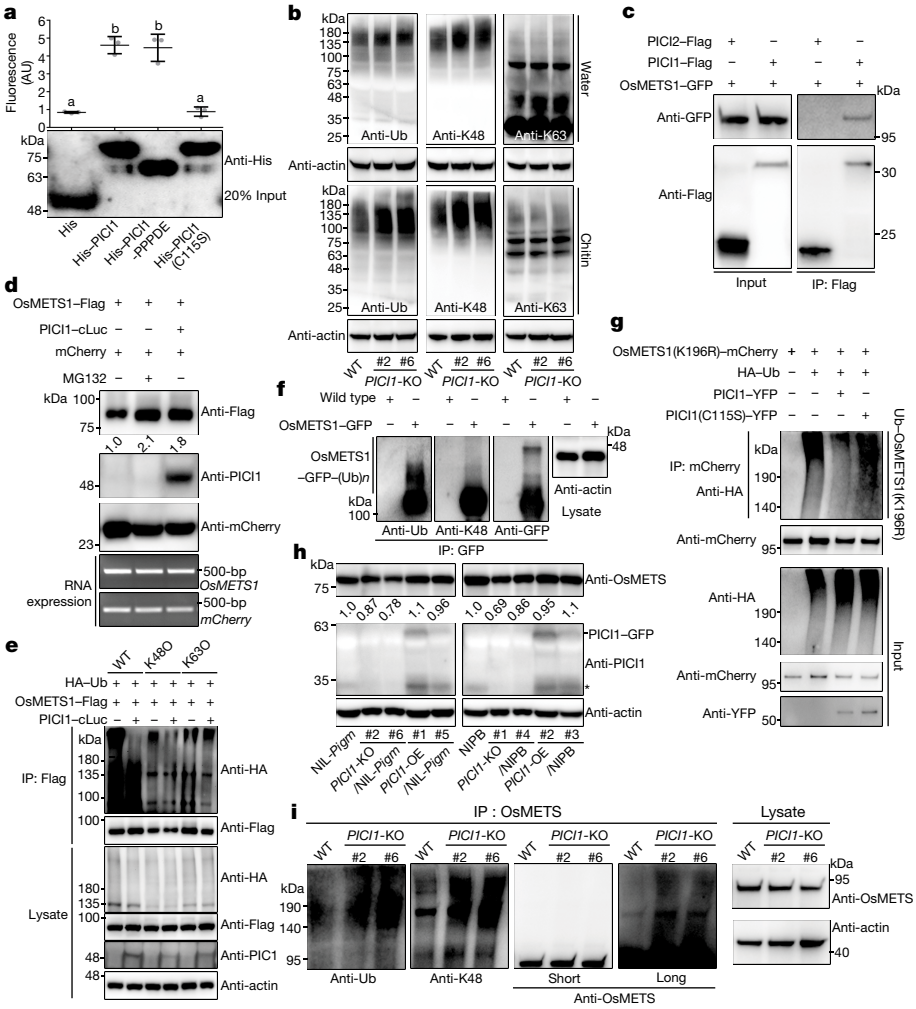

Fig. 2 | PICI1 stabilizes OsMETS through deubiquitination. a, Deubiquitinase activity was observed for His–PICI1 and His–PICI1-PPPDE, but not His–PICI1(C115S). His alone produced from empty vector (pCOLD) served as a negative control. AU, arbitrary units. Lower-case letters indicate statistical significance ($P < 0.05$). One-way ANOVA with Tukey's test. Data are mean ± s.d. ($n = 3$, biologically independent experiments). Exact P values are provided in Supplementary Table 4. **b**, *PICI1*-KO/NIL-*Pigm* showed an increase in ubiquitin conjugates. Total protein extracts from seedlings before (top) or after (bottom) chitin treatment were analysed using anti-ubiquitin (Ub), anti-K48-linked (K48) or anti-K63-linked (K63) ubiquitin chain antibody. WT, NIL-*Pigm*. **c**, Co-IP of OsMETS1–GFP and PICI1–Flag. PICI2 served as a negative control. **d**, Degradation of OsMETS1–Flag in the presence of PICI1 in *N. benthamiana*. MG132 was infiltrated 18 h before sampling. The mCherry tag was expressed as an internal control. The RNA expression of *mCherry* and *OsMETS1* was determined by semi-quantitative PCR. **e**, OsMETS1–Flag was K48-ubiquitin-linked. OsMETS1–Flag and HA–ubiquitin (HA-tagged wild-type, K48O or K63O ubiquitin) were co-expressed with PICI1–cLuc in *N. benthamiana*, and OsMETS1–Flag was immunoprecipitated and detected. **f**, Ubiquitinated OsMETS1–GFP in rice, as revealed by immunoprecipitation and detection. **g**, Deubiquitination of OsMETS1(K196R) by PICI1 but not PICI1(C115S) in rice protoplasts. **h**, Reduced levels of OsMETS in *PICI1*-KO compared with the wild type and *PICI1*-OE in NIPB and NIL-*Pigm*. **i**, Increased ubiquitination of endogenous OsMETS in *PICI1*-KO/NIL-*Pigm* compared with the wild type. Short and long indicate short exposure and long exposure, respectively. Protein abundance was quantified using ImageJ and is indicated under the lanes (**d**, **h**). Actin served as a loading control (**b**, **e**, **f**, **h**, **i**). Experiments were repeated three (**a**, **b**, **d**–**g**) or two (**c**, **h**, **i**) times with similar results.

interaction (Fig. 2c, Extended Data Fig. 4i–k), which showed overlapping subcellular localization (Extended Data Fig. 4l–p). These data strongly suggest that OsMETS1 is a substrate of PICI1.

We measured the accumulation of OsMETS1–Flag in the presence of the 26S proteasome inhibitor MG132 or PICI1-cLuc (Fig. 2d, Extended Data Fig. 4q). Consistently, OsMETS1–Flag degraded faster in *PICI1*-KO/NIL-*Pigm* than in NIL-*Pigm* and *PICI1*-OE/NIL-*Pigm* (Extended Data Fig. 4r). These results suggest that PICI1 stabilizes OsMETS1 in planta. IP–MS analysis of ubiquitinated OsMETS1–GFP revealed four lysine sites that are probably deubiquitinated during infection (Extended Data Fig. 4s, t). Each of the K-R (lysine-arginine substitution) mutants showed enhanced stability compared to wild-type OsMETS1, with K28R being the most stable (Extended Data Fig. 4u, v). Consistently, global ubiquitome profiling revealed decreased ubiquitination of OsMETS1 K28 after PAMP treatment[28]. The chitin-induced expression of pathogen-related genes was substantially increased when individual K-R mutants were expressed (Extended Data Fig. 5a). Moreover, the quadruple mutation further increased OsMETS1 stability (Extended data Fig. 5b, c), implying that the other three lysine residues function additively with K28 to regulate the stability of OsMETS1.

PICI1 deubiquitinates OsMETS

We next co-expressed PICI1–cLuc and OsMETS1–Flag with wild-type, K48O or K63O ubiquitin (the latter indicating ubiquitin with only K48 or K63, respectively). PICI1–cLuc reduced the ubiquitinated OsMETS1–Flag generated with wild-type and K48O ubiquitin, but not K63O ubiquitin (Fig. 2e). Furthermore, OsMETS1–GFP was indeed modulated by K48 ubiquitination (Fig. 2f). Notably, PICI1, but not PICI1(C115S), delayed the

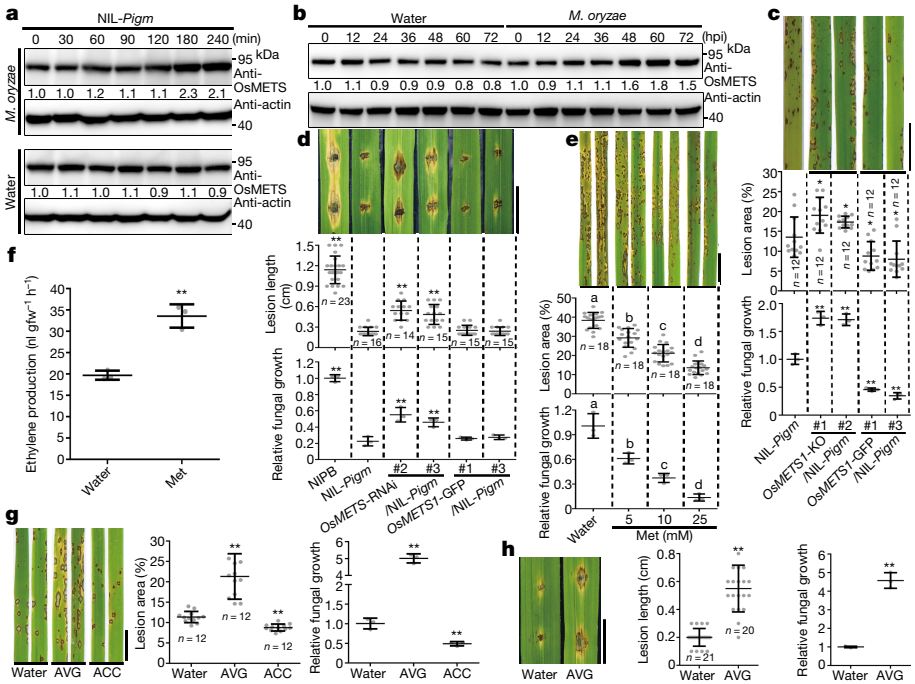

Fig. 3 | Deubiquitination-mediated accumulation of OsMETS enhances blast resistance through promoting Met–ethylene biosynthesis. a, OsMETS accumulation was induced in the early stages of TM21 infection. Water served as a control. **b**, Protein accumulation of OsMETS in NIL-*Pigm* after inoculation with TH12. Relative OsMETS abundance was indicated with actin as a loading control (**a**, **b**). hpi, hours post-infection. **c**, Basal blast resistance of NIL-*Pigm*, *OsMETS1*-KO/NIL-*Pigm* and *OsMETS1* overexpression (*OsMETS1*-GFP/NIL-*Pigm*) lines, 5 dpi using spraying inoculation with TM21. **d**, PigmR-mediated blast resistance, 5 dpi using punch inoculation with TH12. **e**, Increased basal blast resistance after Met application. NIL-*Pigm* seedlings were dipped into different concentrations of Met or water from the roots for 48 h, and inoculated at 7 dpi with TM21. Lower-case letters indicate statistical significance ($P < 0.05$). One-way ANOVA with Tukey's test. Data are mean ± s.d. (lesion areas, $n = 18$, biologically independent samples; fungal growth, $n = 3$, biologically independent samples). **f**, Ethylene content in NIL-*Pigm* after treatment with 25 mM Met or water for 96 h. nl gfw^{-1} h^{-1} indicates the amount of ethylene per gram fresh weight seedling per hour. Two-tailed Student's *t*-test (mean ± s.d.; $n = 3$, biologically independent samples). **g**, Effects of AVG and ACC on basal blast resistance in NIL-*Pigm*. Seedlings were pre-treated with 10 μM AVG, or 20 μM ACC or water for 1 day, then 5 dpi with spraying inoculation (TM21). **h**, Effect of AVG on PigmR-mediated resistance in NIL-*Pigm*, punch-inoculated with TH12 for 5 dpi. For **c**, **d**, **g**, **h**, data were analysed by two-tailed Student's *t*-test. Fungal growth (mean ± s.d.; $n = 3$, biologically independent samples), lesion lengths or areas (mean ± s.d.; n = number of biologically independent samples in the graphs). Scale bars, 1 cm (**c**–**e**, **g**, **h**). Asterisks indicate significant differences (*$P < 0.05$, **$P < 0.01$) (**c**, **d**, **f**–**h**). Exact *P* values are provided in Supplementary Table 4 (**c**–**h**). Experiments were repeated three times with similar results.

degradation of OsMETS1–Flag (Extended Data Fig. 5d), and deubiquitinated OsMETS1(K196R) (Fig. 2g). We used OsMETS1(K196R), as wild-type OsMETS1 is barely detected in rice protoplasts (Extended Data Fig. 4v). An in vitro deubiquitination assay further verified the direct deubiquitination of OsMETS1 by PICI1 (Extended Data Fig. 5e). Collectively, our results suggest that PICI1 deubiquitinates OsMETS1 through cleaving K48-linked ubiquitin.

OsMETS1 shares high similarity with LOC_Os12g42884 (hereafter named OsMETS2) (Extended Data Fig. 5f, g). OsMETS2 also interacted with PICI1, and underwent 26S-proteasome-dependent degradation that was delayed by His–PICI1 (Extended Data Fig. 5h–l), suggesting their functional redundancy. We further confirmed the OsMETS–PICI1 interaction in rice (Extended Data Fig. 5m), and examined endogenous OsMETS (OsMETS1 and OsMETS2) stability using an anti-OsMETS antibody (Fig. 2h, Extended Data Fig. 5n–q). The levels of OsMETS protein, but not mRNA, were lower in *PICI1*-KO than in the wild type and *PICI1*-OE (Fig. 2h, Extended Data Fig. 5r), consistent with the accelerated degradation of OsMETS in *PICI1*-KO (Extended Data Fig. 5n). Moreover, OsMETS was indeed modulated by K48 ubiquitination, which was further enhanced in *PICI1*-KO (Fig. 2i, Extended Data Fig. 5s), confirming that PICI1 cleaves OsMETS K48-linked ubiquitin.

OsMETS functions in PTI and ETI

We first determined that treatment with chitin or flg22 resulted in the accumulation of OsMETS, as was observed for NIL-*Pigm* inoculated with TM21 or *Xoo* at the early stage of infection (Fig. 3a, Extended Data Fig. 6a–c). OsMETS also accumulated after TH12 but not TM21infection in NIL-*Pigm* (Fig. 3b, Extended Data Fig. 6d), implying its ETI function. Of note, TM21-induced accumulation of OsMETS was greatly dampened in *PICI1*-KO, but prolonged in *PICI1*-OE (Extended Data Fig. 6e). Increased deubiquitination of OsMETS1 was also observed in PTI and ETI (Extended Data Fig. 6f, g). The data suggest that PTI and ETI induce the accumulation of OsMETS through PICI1. Furthermore, *OsMETS1*-KO and *OsMETS2*-KO increased, whereas *OsMETS1*-OE and *OsMETS2*-OE decreased, susceptibility to TM21, compared with NIL-*Pigm* (Fig. 3c, Extended Data Figs. 5p, q, 6h–l), suggesting that OsMETS functions in PTI. Slight susceptibility to TH12 was observed in *OsMETS1*-KO and *OsMETS2*-KO (Extended Data Fig. 6m, n), but this was greatly enhanced when RNA interference (RNAi) was used (*OsMETS1*- and *OsMETS2*-RNAi) (Fig. 3d, Extended Data Fig. 6o, p), suggesting the redundant roles of OsMETS1 and OsMETS2 in PigmR-mediated ETI. *OsMETS*-RNAi lines exhibited a dwarf phenotype (Extended Data Fig. 6q, r), with a reduced Met content (Extended Data Fig. 6s). We could not generate *OsMETS1* and *OsMETS2* double-knockout plants, probably owing to the essential role of Met in growth.

We next tested Met-mediated immunity, and observed dose-dependent Met-induced resistance with the induction of pathogen-related genes (Fig. 3e, Extended Data Fig. 6t–v). In addition, Met rescued *OsMETS1*-KO susceptibility, and even enhanced resistance, similar to *OsMETS* overexpression (Extended Data Fig. 6w). Likewise, *PICI1*-KO

decreased Met content, and Met supplementation restored its resistance (Extended Data Fig. 6x, y). In addition, fungal growth was inhibited by 10 and 25 mM but not by 5 mM Met (Extended Data Fig. 7a)—which are much higher concentrations than that seen in rice—suggesting Met-mediated immune activation. Together, these results show that OsMETS-mediated biosynthesis of Met has an important role in blast resistance.

OsMETS functions through ethylene

Met is the precursor of ethylene functioning in plant immunity[9]. Indeed, treatment with Met increased the production of ethylene (Fig. 3f). Of note, PTI-induced ethylene production was significantly decreased in *OsMETS1*-KO and *PICI1*-KO, whereas it was increased in *OsMETS1*-OE and *PICI1*-OE (Extended Data Fig. 7b, c). Treatment with ethylene led to the downregulation of *OsMETS1* and *OsMETS2* (Extended Data Fig. 7d–f), suggesting negative feedback regulation. Pre-treatment with ACC (1-aminocyclopropane-1-carboxylic acid, an ethylene precursor) decreased, whereas AVG (aminoethoxyvinylglycine, an ethylene biosynthesis inhibitor) increased, blast susceptibility (Fig. 3g, Extended Data Fig. 7g, h). In addition, ACC rescued *OsMETS*-RNAi and *PICI1*-KO resistance (Extended Data Fig. 7i, j), indicating that ethylene is involved in PICI1–OsMETS-mediated PTI. Notably, pre-treatment with AVG resulted in compromised resistance of NIL-*Pigm* to TH12, suggesting that ethylene is also critical to PigmR-mediated ETI (Fig. 3h). *OsACS2*, a key ethylene biosynthesis enzyme, was activated during PTI and ETI, with increased ethylene production (Extended Data Fig. 7k–m). Consistently, *OsACS2*-KO decreased basal blast resistance (Extended Data Fig. 7o). However, PigmR-mediated ETI was not affected in *OsACS2*-KO (Extended Data Fig. 7p), suggesting that ETI disturbance may need more deprivation of ethylene owing to the functional redundancy of *OsACS* proteins[29]. Therefore, ethylene is actively involved in blast resistance. We further observed that AVG treatment could partially dampen the Met-induced resistance (Extended Data Fig. 7q), suggesting that ethylene biosynthesis is a major function of Met in immune activation.

PigmR protects PICI1 from effectors

To elucidate the mechanism of PICI1 function in PigmR-mediated resistance, we analysed the levels of PICI1 during blast infection. PICI1 protein, but not mRNA, increased in NIL-*Pigm* inoculated with avirulent TH12, whereas PICI1 gradually declined in NIPB and NIL-*Pigm* inoculated with virulent strains (Extended Data Fig. 7r, s). The results strongly suggest that fungal effectors are involved in PICI1 turnover. We therefore screened 10 known blast effectors for direct interactions with PICI1, and found that PICI1 bound to 5 of these effectors—AvrPizt[20], AvrPii[19], AvrPia[19], AvrPWL2[17] and AvrPi9[18]—with a higher affinity than to AvPikC[16] and AvrPikD[16], whereas AvrBAS4[13], AvrSlp1[14], AvrPita[15] or MBP tag were not pulled down with PICI1 (Extended Data Fig. 8a). Furthermore, an SLC assay suggested that PICI1 interacted with AvrPi9, AvrPWL2 and AvrPii with a similar or higher binding affinity to the known AvrPii–OsNADP–ME2[30], but with a lower affinity to that of AvrPikD-HMA[31,32] in planta (Extended Data Fig. 8b–d). Moreover, these effectors interacted specifically with PICI1 but not PICI2 (Extended Data Fig. 8e–g), suggesting that PICI1 is a unique immune hub that is co-opted by various effectors. AvrPizt and AvrPia may not interact with PICI1 in planta, probably owing to altered subcellular localization, conformation or modification.

We then generated Avr-expressing transgenic plants and found that AvrPi9—but not AvrPizt, AvrPWL2 or AvrPii—reduced the endogenous levels of PICI1 (Extended Data Fig. 8h). In addition, AvrPi9, but not AvrPizt, co-localized with PICI1 (Fig. 4a, Extended Data Fig. 8i, j). Co-immunoprecipitation and bimolecular fluorescence complementation (BiFC) further specified the AvrPi9–PICI1 interaction (Fig. 4b, Extended Data Fig. 8k). Notably, ectopic expression of *AvrPi9* led to enhanced susceptibility with decreased expression of pathogen-related genes (Extended Data Fig. 8l–n), indicating that AvrPi9 suppresses rice PTI. We also found that AvrPi9–mCherry—but not mCherry, AvrPizt–mCherry or AvrPWL2–mCherry—promoted the degradation of PICI1–GFP (Fig. 4c, Extended Data Fig. 8o). Consistently, the endogenous PICI1 exhibited faster degradation in AvrPi9-containing versus AvrPWL2-containing plants (Fig. 4d), which was not affected by MG132 (Fig. 4d, Extended Data Fig. 8p), suggesting non-26S proteasome degradation.

Of note, the AvrPi9-mediated degradation of PICI1–GFP was delayed in PICI1–GFP/NIL-*Pigm* compared to PICI1–GFP/NIPB (Extended Data Fig. 8p), suggesting that PigmR protects PICI1 from degradation by AvrPi9. To test this, we first determined that PICI1 decreased to a greater extent after overexpression of AvrPi9 in NIPB versus NIL-*Pigm* (Fig. 4e). Infection with TH12 (without AvrPi9) or TH12^{AvrPi9} (containing AvrPi9) increased PICI1 in NIL-*Pigm* but decreased PICI1 in NIPB at a faster rate with TH12^{AvrPi9} versus TH12 inoculation (Extended Data Fig. 8q–s), suggesting that PICI1 is hijacked by AvrPi9 and other as-yet-unidentified effectors, but protected by PigmR. AvrPi9 is the Avr effector of Pi9, and PigmR is neither activated nor induced in an AvrPi9-dependent manner (Extended Data Fig. 9a–c), suggesting that immune-active PigmR interferes with the AvrPi9–PICI1 interaction to inhibit the degradation of PICI1. Indeed, the AvrPi9-triggered degradation of PICI1–GFP was greatly delayed by avirulent infection (Fig. 4f), accompanied by enhanced PigmR–PICI1 interaction (Extended Data Fig. 9d). AvrPi9–PICI1 interaction was reduced in the presence of PigmR or the coiled-coil domain of PigmR (PigmR-CC) (Extended Data Fig. 9e–h). PigmR-CC also protects PICI1 from AvrPWL2 and AvrPii binding (Extended Data Fig. 9i–l), suggesting that this competitive mechanism might be widely used by PigmR.

We further found that PICI1 and OsMETS accumulated in *Pizt* and *Pi9* plants during avirulent strain infection (Extended Data Fig. 9m, n), and that this PICI1 induction was absent in *Pizt*-KO/ZH11 (Extended Data Fig. 9o). Pizt-CC can also protect PICI1 from AvrPi9, AvrPWL2 and AvrPii binding in planta (Extended Data Fig. 9p). These results suggest that PICI1 is likely to be protected in general by NLRs.

PICI1 alleles confer immune divergence

Notably, using NIPB as the reference in the 3,000 Rice Genome Project[33], 27 single-nucleotide polymorphisms (SNPs) were identified in its promoter, nearly all of which are within *indica* germplasm (hereafter named *ProPICI1^{ind}*), together with some *aus*, *admix* and *aro* accessions (Extended Data Fig. 10a, Supplementary Table 2); by contrast, the majority of *japonica* varieties are the *ProPICI1^{NIPB}* haplotype (hereafter named *ProPICI1^{jap}*) (Extended Data Fig. 10b, Supplementary Table 2). Among the 27 SNPs, 13 SNPs are well correlated with *indica–japonica* differentiation, which was verified in 96 global rice collections[34] (Fig. 4g, Supplementary Table 2), implying that *PICI1* is differentially expressed between *indica* and *japonica*. The decreased nucleotide diversity (π) of the *PICI1* promoter in the *indica* and *japonica* subspecies compared with that in wild rice (*Oryza rufipogon*) (Fig. 4h) suggests a selection during domestication. Moreover, fixation index (F_{ST}) analysis revealed a greater genetic distance between *indica* and *japonica* (Extended Data Fig. 10c), suggesting divergent *indica–japonica* domestication.

We found that *ProPICI1^{jap}* showed higher transcriptional activity than *ProPICI1^{ind}* after treatment with chitin (Extended Data Fig. 10d), consistent with higher fungal induction of *PICI1* in *japonica* than in *indica* (Extended Data Fig. 10e). Furthermore, a chromosome segment substitution line (CSSL) containing the *PICI1^{jap}* allele in Huajingxian74 (*ProPICI1^{ind}*) exhibited an increase in *PICI1* induction compared with Huajingxian74 (Extended Data Fig. 10f, g, Supplementary Table 2), indicating that the SNPs are likely to regulate *PICI1* expression. In addition, we detected higher basal defence in the CSSL (Fig. 4i, Extended Data Fig. 10f, h). These data are consistent with and may explain previous findings that *japonica* has higher levels of Met[35] and higher field and basal blast resistance than *indica*[36]. Collectively, our results suggest that *PICI1* contributes to subspecies divergence in basal defence, thus providing a potential breeding target for broad-spectrum blast resistance together with NLRs in rice.

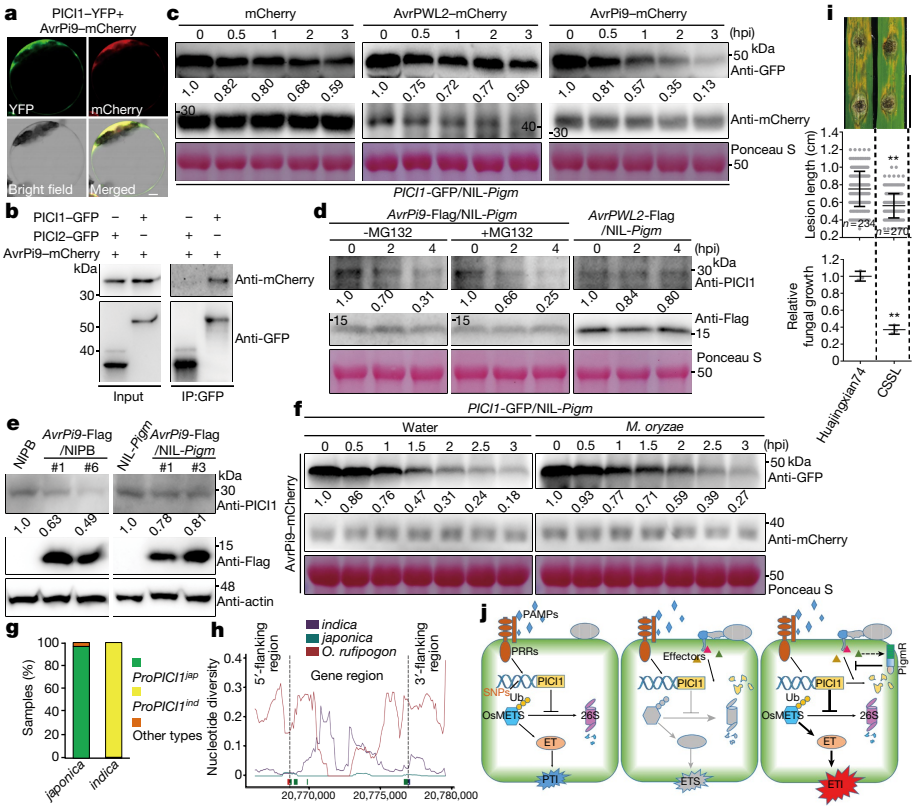

Fig. 4 | PigmR protects PICI1 from degradation by AvrPi9, and natural variation in *PICI1* contributes to subspecies immune divergence. **a**, Co-localization of PICI1–YFP and AvrPi9–mCherry in rice protoplasts. Scale bar, 5 μm. **b**, PICI1–GFP but not PICI2–GFP interacts with AvrPi9–mCherry in co-IP. **c**, Cell-free assay shows AvrPi9-mediated degradation of PICI1–GFP. PICI1–GFP/NIL-*Pigm* extracts were incubated with AvrPi9–mCherry expressed in *N. benthamiana*. mCherry and AvrPWL2–mCherry served as negative controls. **d**, AvrPi9 promotes endogenous PICI1 degradation independently of the 26S proteasome in a rice cell-free assay. *AvrPWL2*-Flag/NIL-*Pigm* served as a control. **e**, Reduced levels of PICI1 in *AvrPi9*-Flag/NIPB and *AvrPi9*-Flag/NIL-*Pigm* compared with the wild type. **f**, PICI1–GFP degradation is delayed in infected NIL-*Pigm*. *PICI1*-GFP/NIL-*Pigm* extracts inoculated with TH12 or water (36 hpi) were incubated with AvrPi9–mCherry expressed in *N. benthamiana*. **g**, Percentages of *ProPICI1*^{jap} and *ProPICI1*^{ind} haplotypes in subspecies *japonica* and *indica*. **h**, Nucleotide diversity (π) of *PICI1* and flanking regions in *indica*, *japonica* and wild rice (*O. rufipogon*). **i**, Basal blast resistance of Huajingxian74 and CSSL plants to the virulent isolate YN2, 5 dpi. Scale bar, 1 cm. Two-tailed Student's *t*-test. Fungal growth (mean ± s.d.; $n = 3$, biologically independent samples), lesion lengths (mean ± s.d.; n = numbers of biologically independent samples in the graph). Asterisks indicate significant differences (**$P < 0.01$). Exact P values are provided in Supplementary Table 4. **j**, Proposed model for the NLRs–PICI1–OsMETS–ethylene (ET) immune cascade. PICI1 is targeted by both NLRs and Avr effectors, and induced by PAMPs to initiate PTI. Activated NLRs protect PICI1 from effector-mediated degradation to reboot the Met–ethylene biosynthesis, resulting in robust defence through integrating PTI and ETI. Protein abundance was quantified using ImageJ and is indicated under the lanes (**c**–**f**). Ponceau S staining (**c**, **d**, **f**) or actin (**e**) served as loading controls. Experiments were repeated twice (**b**, **e**) or three times (**a**, **c**, **d**, **f**, **i**) with similar results.

Discussion

We have thus revealed here an NLR–effector arms race that controls the biosynthesis of primary metabolites and immune activation in rice. Rice NLRs including PigmR and blast effectors including AvrPi9 both target PICI1, which stabilizes OsMETS to promote Met–ethylene biosynthesis (Fig. 4j). Therefore, we propose that NLRs counteract effectors to ensure efficient immunity with a 'competitive' mode. It would be worth investigating whether the same mechanism is adopted in other pathosystems. The PICI1–OsMETS–ethylene cascade is used in both PTI and ETI, and this ETI–PTI integration contributes to broad-spectrum blast resistance mediated by PigmR and other similar NLRs. However, we cannot exclude roles for other Met derivatives or Met-related processes in blast resistance.

PICI1 is probably hijacked to suppress host immunity by multiple pathogen effectors, similarly to *Arabidopsis* RIN4[37,38]. Indeed, we observed specific acetylation of K160 in PICI1 after infection (Extended Data Fig. 10i, j, Supplementary Table 1), which promoted the degradation of PICI1—as a PICI1 acetyl-lysine mimic mutant was unstable—and thus weakened interactions with OsMETS1 and PigmR (Extended Data Fig. 10k). How PICI1 is subjected to differential modifications by diverse effectors needs to be further elucidated. However, we suggest that the NLR–PICI1 surveillance mechanism could provide a strategy for breeding disease-resistant crops.

Online content

Any methods, additional references, Nature Research reporting summaries, source data, extended data, supplementary information, acknowledgements, peer review information; details of author contributions and competing interests; and statements of data and code availability are available at https://doi.org/10.1038/s41586-021-04219-2.

1. Jones, J. D. & Dangl, J. L. The plant immune system. *Nature* **444**, 323–329 (2006).
2. Couto, D. & Zipfel, C. Regulation of pattern recognition receptor signalling in plants. *Nat. Rev. Immunol.* **16**, 537–552 (2016).
3. Xin, X.-F. Kvitko, B. & He, S. Y. *Pseudomonas syringae*: what it takes to be a pathogen. *Nat. Rev. Microbiol.* **16**, 316–328 (2018).
4. Kourelis, J. & van der Hoorn, R. A. L. Defended to the nines: 25 years of resistance gene cloning identifies nine mechanisms for R protein function. *Plant Cell* **30**, 285–299 (2018).
5. Li,W., Deng, Y., Ning, Y., He, Z. & Wang, G. L. Exploiting broad-spectrum disease resistance in crops: from molecular dissection to breeding. *Annu. Rev. Plant Biol.* **71**, 575–603 (2020).

6. Ngou, B. P. M., Ahn, H.-K., Ding, P. & Jones, J. D. G. Mutual potentiation of plant immunity by cell-surface and intracellular receptors. *Nature* **592**, 110–115 (2021).
7. Yuan, M. et al. Pattern-recognition receptors are required for NLR-mediated plant immunity. *Nature* **592**, 105–109 (2021).
8. Bürger, M. & Chory, J. Stressed out about hormones: how plants orchestrate immunity. *Cell Host Microbe* **26**, 163–172 (2019).
9. Broekaert, W. F., Delauré Sl, M. F. C., Bolle, D., De Bolle, Mf, B. P. A. & Cammue, B. P. The role of ethylene in host-pathogen interactions. *Annu. Rev. Phytopathol.* **44**, 393–416 (2006).
10. Washington, E. J. et al. *Pseudomonas syringae* type III effector HopAF1 suppresses plant immunity by targeting methionine recycling to block ethylene induction. *Proc. Natl Acad. Sci. USA* **113**, E3577–E3586 (2016).
11. Zhao, S. et al. A viral protein promotes host SAMS1 activity and ethylene production for the benefit of virus infection. *eLife* **6**, e27529 (2017).
12. Dean, R. et al. The top 10 fungal pathogens in molecular plant pathology. *Mol. Plant Pathol.* **13**, 414–430 (2012).
13. Mosquera, G., Giraldo, M. C., Khang, C. H., Coughlan, S. & Valent, B. Interaction transcriptome analysis identifies *Magnaporthe oryzae* BAS1–4 as biotrophy-associated secreted proteins in rice blast disease. *Plant Cell* **21**, 1273–1290 (2009).
14. Mentlak, T. A. et al. Effector-mediated suppression of chitin-triggered immunity by *Magnaporthe oryzae* is necessary for rice blast disease. *Plant Cell* **24**, 322–335 (2012).
15. Orbach, M. J., Farrall, L., Sweigard, J. A., Chumley, F. G. & Valent, B. A telomeric avirulence gene determines efficacy for the rice blast resistance gene *Pi-ta*. *Plant Cell* **12**, 2019–2032 (2000).
16. Kanzaki, H. et al. Arms race co-evolution of *Magnaporthe oryzae AVR-Pik* and rice *Pik* genes driven by their physical interactions. *Plant J.* **72**, 894–907 (2012).
17. Sweigard, J. A. et al. Identification, cloning, and characterization of PWL2, a gene for host species-specificity in the rice balst fungus. *Plant Cell* **7**, 1221–1233 (1995).
18. Wu, J. et al. Comparative genomics identifies the *Magnaporthe oryzae* avirulence effector AvrPi9 that triggers Pi9-mediated blast resistance in rice. *New Phytol.* **206**, 1463–1475 (2015).
19. Yoshida, K. et al. Association genetics reveals three novel avirulence genes from the rice blast fungal pathogen *Magnaporthe oryzae*. *Plant Cell* **21**, 1573–1591 (2009).
20. Li, W. et al. The *Magnaporthe oryzae* avirulence gene *AvrPiz-t* encodes a predicted secreted protein that triggers the immunity in rice mediated by the blast resistance gene *Piz-t*. *Mol. Plant Microbe Interact.* **22**, 411–420 (2009).
21. Deng, Y. et al. Epigenetic regulation of antagonistic receptors confers rice blast resistance with yield balance. *Science* **355**, 962–965 (2017).
22. Xie, Z. et al. A nucleotide-binding site-leucine-rich repeat receptor pair confers broad-spectrum disease resistance through physical association in rice. *Phil. Trans. R. Soc. B* **374**, 20180308 (2019).
23. Zhou, B. et al. The eight amino-acid differences within three leucine-rich repeats between *Pi2* and *Piz-t* resistance proteins determine the resistance specificity to *Magnaporthe grisea*. *Mol. Plant Microbe Interact.* **19**, 1216–1228 (2006).
24. Xie, X. et al. PPPDE1 promotes hepatocellular carcinoma development by negatively regulate p53 and apoptosis. *Apoptosis* **24**, 135–144 (2019).
25. Shimizu, T. et al. Two LysM receptor molecules, CEBiP and OsCERK1, cooperatively regulate chitin elicitor signaling in rice. *Plant J.* **64**, 204–214 (2010).
26. Suh, H. Y. et al. Crystal structure of DeSI-1, a novel deSUMOylase belonging to a putative isopeptidase superfamily. *Proteins* **80**, 2099–2104 (2012).
27. Komander, D. & Rape, M. The ubiquitin code. *Annu. Rev. Biochem.* **81**, 203–229 (2012).
28. Chen, X. L. et al. Proteomic analysis of ubiquitinated proteins in rice (*Oryza sativa*) after treatment with pathogen-associated molecular pattern (PAMP) elicitors. *Front. Plant Sci.* **9**, 1064 (2018).
29. Iwai, T., Miyasaka, A., Seo, S. & Ohashi, Y. Contribution of ethylene biosynthesis for resistance to blast fungus infection in young rice plants. *Plant Physiol.* **142**, 1202–1215 (2006).
30. Singh, R. et al. Magnaporthe oryzae effector AVR-Pii helps to establish compatibility by inhibition of the rice NADP-malic enzyme resulting in disruption of oxidative burst and host innate immunity. *Mol. Cells* **39**, 426–438 (2016).
31. De la Concepcion, J. C. et al. Polymorphic residues in rice NLRs expand binding and response to effectors of the blast pathogen. *Nat. Plants* **4**, 576–585 (2018).
32. Maqbool, A. et al. Structural basis of pathogen recognition by an integrated HMA domain in a plant NLR immune receptor. *eLife* **4**, 08709 (2015).
33. Wang, W. et al. Genomic variation in 3,010 diverse accessions of Asian cultivated rice. *Nature* **557**, 43–49 (2018).
34. Huang, X. et al. Genome-wide association study of flowering time and grain yield traits in a worldwide collection of rice germplasm. *Nat. Genet.* **44**, 32–39 (2011).
35. Hu, C. et al. Metabolic variation between *japonica* and *indica* rice cultivars as revealed by non-targeted metabolomics. *Sci. Rep.* **4**, 5067 (2014).
36. Liao, J. et al. Pathogen effectors and plant immunity determine specialization of the blast fungus to rice subspecies. *eLife* **5**, e19377 (2016).
37. Axtell, M. J. & Staskawicz, B. J. Initiation of *RPS2*-specified disease resistance in *Arabidopsis* is coupled to the AvrRpt2-directed elimination of RIN4. *Cell* **112**, 369–377 (2003).
38. Mackey, D., Holt, B. F. III, Wiig, A. & Dangl, J. L. RIN4 interacts with *Pseudomonas syringae* type III effector molecules and is required for RPM1-mediated resistance in *Arabidopsis*. *Cell* **108**, 743–754 (2002).

Methods

Plant materials and growth conditions

The *japonica* variety Nipponbare (NIPB) and near-isogenic *Pigm* line (NIL-*Pigm*), *OsCERK1*-KO/NIPB, *Pizt*-KO/ZH11 and *PigmR-7Myc-6His*/NIPB used in this study were collected or generated in our previous study[21,22,39]. Huajingxian74 and the CSSL were provided by G. Zhang. The following transgenic lines were developed in this study: *PICI1*-KO/NIPB, *PICI1*-KO/NIL-*Pigm*, *PICI1*-OE(*pUBI::PICI1-GFP*)/NIPB, *PICI1*-Flag(*pUBI::PICI1-Flag*)/NIPB, *PICI2*-Flag(*pUBI::PICI2-Flag*)/NIPB, *PICI1*-OE(*pUBI::PICI1-GFP*)/NIL-*Pigm*, *OsMETS1*-KO/NIL-*Pigm*, *OsMETS2*-KO/NIL-*Pigm*, *OsMETS1*-OE(*pUBI::OsMETS1-GFP*)/NIL-*Pigm*, *OsMETS2*-OE(*pUBI::OsMETS2-GFP*)/NIL-*Pigm*, *OsMETS*-RNAi/NIL-*Pigm*, *OsACS2*-KO/NIL-*Pigm*, *OsCERK1*-KO/*PICI1*-KO/NIPB, *OsCERK1*-KO/*PICI1*-OE/NIPB, *PICI1*-KO/ZH11, *PICI1*-KO/Ky-*Pi9*, *AvrPi9-Flag*/NIL-*Pigm*, *AvrPi9-Flag*/NIPB, *AvrPWL2-Flag*/NIL-*Pigm*, *AvrPii-Flag*/NIL-*Pigm* and *AvrPizt-Flag*/NIL-*Pigm*. Rice plants were grown in the experimental fields in Shanghai for the summer season, or Lingshui, Hainan for the winter season under natural field conditions for plant inoculation (punch injection) and seed production. For seedling spraying inoculation, two-week-old seedlings were grown at the greenhouse at 26 °C, 14-h day–10-h night. *Nicotiana benthamiana*, used for transient expression, protein–protein interaction and degradation analysis, was grown at the greenhouse at 22 °C under long-day conditions (16-h day–8-h night).

Development of transgenic rice plants

For CRISPR–Cas9 constructs, the designed target sequences of *PICI1*, *OsMETS1*, *OsMETS2* and *OsACS2* were synthesized and CRISPR–Cas9 constructs were generated following the protocol reported[40]. To generate constructs for *PICI1*, *PICI2*, *OsMETS1/2*, *AvrPi9*, *AvrPWL2*, *AvrPii* and *AvrPizt* fusion overexpression, the corresponding coding sequences were inserted into PUN1301-*pUBI-GFP* or PUN1301-*pUBI-Flag* vectors. To generate the *OsMETS* RNAi construct, a conserved 540-bp coding sequence fragment of *OsMETS* was selected and inserted as inverted repeats into the RNAi vector PTCK303. The CRISPR–Cas9, RNAi and overexpression plasmids were introduced into NIL-*Pigm*, ZH11, Ky-*Pi9* or NIPB via *Agrobacterium* (EHA105)-mediated transformation to generate more than 20 independent transgenic lines for each construct, further selected by PCR-based sequencing or western blot. All primer sequences used for cloning can be found in Supplementary Table 3.

Y2H screen and assay

The Y2H screen was conducted to identify the PigmR-interacting candidates as previously described[41]. In brief, the truncated N-terminal part (CC domain) of PigmR was fused to the GAL4 DNA-binding domain in pDEST32 as the bait to screen the rice cDNA library in pDEST22 according to the manufacturer's instructions (Invitrogen), with yeast strain AH109. Positive clones were screened and sequenced.

For the Y2H assay, the target coding sequences were cloned into pDEST22(AD) or pDEST32(BD) vectors. Different construct combinations were co-transformed into yeast strain AH109 and clones were grown on selective medium (lacking Trp, Leu and His) containing proper 3-aminotriazole to test the protein–protein interaction. Images were taken 3 days after incubation at 30 °C.

Rice blast inoculation

Rice blast inoculation was performed as usual[21,41]. In brief, *M. oryzae* spores were collected in sterile water containing 0.05% Tween-20 and the spore concentration was adjusted to approximately 1×10^5 spores per ml for spraying, punch injection or punch inoculation. For spray inoculation, two-week-old seedlings were sprayed with spore suspensions in a dew growth chamber. Leaves of tillering plants grown in the field were punch-injection-inoculated or punch-inoculated as previously described[41]. At 5–7 dpi, lesions were evaluated by calculating lesion areas and lengths using the software ImageJ or a ruler. Relative fungal growth was measured by DNA-based quantitative PCR (qPCR) using the threshold cycle value (C_T) of *M. oryzae* 28S *rDNA* against the C_T of rice genomic *ACTIN1* DNA.

SLC, BiFC and subcellular localization

The SLC and BiFC assays were described previously[41]. For SLC assays, the tested coding sequences were cloned into pCAMBIA-35S-nLuc or pCAMBIA-35S-cLuc, and the resulting plasmids were transformed into *Agrobacterium* (strain GV3101), cultured overnight in LB medium, collected and suspended in infiltration buffer (10 mM $MgCl_2$, 10 mM methylester sulfonate, 150 μM acetosyringone, pH 5.6), and incubated for 2–3 h at 30 °C before infiltration. The suspensions were then infiltrated into 5-week-old *N. benthamiana* leaves in different combinations. After two days of growth, luciferase substrate (Promega) was sprayed onto the surface of the leaves and the luciferase signals were imaged using a Tanon-5200 imaging system (Tannon). For luciferase activity measurement, leaves were taken and ground into fine powder in liquid nitrogen, homogenized in the lysis buffer following the manufacturer's instructions (Promega). The extraction solution was then incubated with luciferin substrate in a 96-well plate for 10–15 min, and luminescence was captured with the Varioskan Flash (Thermo Fisher Scientific) plate reader. For the BiFC assay in rice protoplasts, the PICI1, PigmR-CC, Pish-CC, PICI2 and AvrPi9 coding sequences were inserted into PSAT1-nVenus or PSAT1-cCFP, respectively. Different construct combinations were co-expressed in rice protoplasts prepared from seedling sheaths. Fluorescence images were recorded on a confocal microscope (Olympus Fluoview FV1000) at 16 h after transformation.

For subcellular localization of proteins in rice protoplasts, the coding sequences of PICI1, OsMETS1, PigmR, AvrPi9 and AvrPizt were inserted into PA7-35S-YFP or pAN583-35S-mCherry, respectively. The fusion constructs were transformed alone or co-transformed into rice protoplasts. The NLS sequence was fused in-frame with RFP into PA7-35S-RFP as a nuclear marker. Fluorescence was detected using a confocal microscope (Olympus Fluoview FV1000) after incubation in the dark for 16–20 h at 26 °C. To visualize the subcellular localization of PICI1–GFP or OsMETS1–GFP in transgenic rice root, the root tips were stained with 10 μM DAPI for 5 min before capturing the images using a confocal microscope (Olympus Fluoview FV1000).

ROS measurement

For measurement of ROS bursts in rice cells after chitin treatment, the luminol chemiluminescence assay was conducted as described previously with some modifications[42]. In brief, leaf sheaths from 10-day-old rice plants cultivated in 1/2 MS medium were cut (approximately 3-mm strips) and preincubated overnight in sterile distilled water to recover from wounding stress. The materials were then treated with 1×10^{-6} M chitin [octa-*N*-acetylchitooctaose $(GlcNAc)_8$], 1×10^{-6} M flg22 or water as a control in reaction buffer containing 20 μM luminol (Wako) and 10 μg ml^{-1} horseradish peroxidase (Sigma). Immediately after the treatment, luminescence was monitored continuously at 10-s intervals for 25 min with a Glomax 20/20 luminometer (Promega) or 1-min intervals for 40 min with a Varioskan Flash multireader (Thermo Fisher Scientific).

Cell-free degradation assay

For the cell-free protein degradation assay, total proteins were extracted from rice seedlings or *N. benthamiana* leaves with the extraction buffer (50 mM Tris-MES, pH 8.0, 0.5 M sucrose, 1 mM $MgCl_2$, 10 mM EDTA, 5 mM dithiothreitol, 1 mM phenylmethylsulfonyl fluoride and 1× protease inhibitor cocktail). Samples were incubated at 25 °C with or without 50 μM MG132 and taken at the indicated intervals for the western blotting. All protein immunodetection experiments were performed independently three times with similar results.

Protein extraction, immunoblotting and co-immunoprecipitation

The PICI1 and OsMETS polyclonal antibodies were custom-developed by ABclonal Technology. The PICI1 (100–246 aa) and OsMETS (410–766 aa) proteins were expressed, purified and used as antigens to raise polyclonal antibodies in rabbit.

To extract total proteins from plants, 0.2 g of fresh leaves or rice seedling sheaths were ground into fine powder in liquid nitrogen, homogenized in the protein extraction buffer (150 mM Tris-HCl, pH 7.5, 6 M urea, 2% SDS, and 5% β-mercaptoethanol), boiled for 5 min and then centrifuged at 16,000*g* for 10 min at 4 °C to remove debris. Supernatants were collected with SDS loading buffer for protein gel blot. For total protein extraction from yeast, a post-alkaline extraction method was performed. In brief, yeast cells are collected, resuspended in 100 µl 0.2 M NaOH, incubated for 5 min at room temperature, then pelleted and resuspended in 50 µl SDS loading buffer, followed by boiling for 5 min, and the resulting supernatants were separated using SDS–PAGE.

The co-immunoprecipitation (co-IP) procedure was described previously[41]. Protein extracts from *N. benthamiana* or rice leaves were prepared in the IP extraction buffer (50 mM Tris-HCl, pH 7.5, 150 mM NaCl, 1 mM EDTA, 10% glycerol, 1% Triton X-100, 1 mM PMSF and 1× protease inhibitor cocktail). Different combinations of supernatants were incubated with anti-Myc beads, anti-Flag beads or anti-GFP beads for 2 h at 4 °C and then washed four times with extraction buffer. The bound proteins were eluted from the affinity beads by boiling for 5 min in SDS loading buffer and analysed by western blot.

Quantification of protein accumulation was performed using ImageJ software. Antibodies against the following proteins were used: Myc (1:2,000), GFP (1:2,000), PICI1 (1:1,000), His (1:1,000), MBP (1:1,000), ubiquitin (1:1,000), K48-linkage ubiquitin (1:1,000), K63-linkage ubiquitin (1:1,000), Ac-K-103 (1:1,000), Flag (1:2,000), GAL4-AD (1:1,000), GAL4-BD (1:1,000), mCherry (1:1,000), nLuc (1:1,000), S-tag (1:1,000), HA (1:1,000), OsMETS (1:1,000), actin (1:2,000), goat anti-rabbit IgG secondary antibody (1:10,000) and goat anti-mouse IgG secondary antibody (1:10,000).

Recombinant protein preparation and pull-down assay

To construct His-fusion plasmids for the production of recombinant proteins, the coding sequences were PCR-amplified and inserted into pCOLD (His–PICI1, His–PICI1-PPPDE, His–PICI1(C115S), His–OsMETS1, His–OsMETS1-2, His–OsMETS1(K28R), His–OsMETS1(K196R), His–OsMETS1(K458R) and His–OsMETS1(K740R)). All protein site mutations were generated by mutagenesis kit following the manufacturer's instructions. The recombinant proteins were produced in the *Escherichia coli* strain Rosetta (DE3) and induced with 0.5 mM isopropyl β-D-thiogalactoside (IPTG) for 20 h at 18 °C. Bacterial cells were collected and affinity-purified with Ni-NTA agarose (QIAGEN) following the manufacturer's instructions. To identify the recombinant protein purity and concentration, Coomassie brilliant blue R-250 staining with quantified BSA as a standard was performed. For pull-down assays, bait proteins were captured with corresponding resin (Amylose Resin for MBP-tagged Avr proteins or glutathione sepharose 4B for GST-tagged PICI1), washed three times, then incubated with prey proteins at 4 °C for 2 h in binding buffer (50 mM Tris-HCl, pH 7.5, 100 mM NaCl, 10% (v/v) glycerol). The beads were then washed twice or three times with the washing buffer (50 mM Tris-HCl, pH 7.5, 100 mM NaCl, 10% (v/v) glycerol, 0.1% (v/v) Triton X-100) to remove non-specifically bound proteins, and the precipitates were released by boiling in SDS sample buffer at 100 °C for 5 min and detected by immunoblotting using corresponding antibodies. All PCR primers are listed in Supplementary Table 3.

Deubiquitination assay

Ubiquitin 7-amido-4-methylcoumarin (ubiquitin-AMC, Enzo) was used as a substrate to monitor the enzymatic activity of ubiquitin C-terminal hydrolase (UCH), which releases the fluorogenic AMC component by cleaving the bond between the C-terminus of ubiquitin and AMC. In brief, 1-µg aliquots of recombinant His–PICI1, His–PICI1-PPPDE or His–PICI1(C115S) were incubated with 250 nM ubiquitin-AMC in reaction buffer (50 mM HEPES, pH 7.8, 0.5 mM EDTA and 1 mM dithiothreitol) in a total volume of 100 µl for 1 h. The fluorescence of an AMC moiety was monitored by spectrofluorometry using a Varioskan Flash (Thermo Fisher Scientific) at 380 nm excitation/460 nm emission. For K48-, K63- or linear linked tetra-ubiquitin cleavage assay, recombinant His–PICI1 or His–PICI1-PPPDE was added to 20 µl reaction buffer containing 2.5 µg of K48-, K63- or linear tetra-ubiquitin and held for 1 h at 37 °C. The reactions were stopped by adding SDS loading buffer, followed by separation on SDS–PAGE. Recombinant His alone (pCOLD) was used as a negative control.

RNA analysis

Total RNAs were extracted using TRIzol reagent (Invitrogen) from rice tissues or *N. benthamiana* leaves. For quantitative PCR with reverse transcription (qRT–PCR) or semi-quantitative PCR, total RNA (around 1 µg) was converted into cDNA using ReverTra Ace qPCR RT Master Mix with the gDNA Remover kit according to the manufacturer's instructions (TOYOBO). The qRT–PCR reaction was performed using a CFX96 Real-time PCR Instrument (Bio-Rad) with SYBR Premix Ex Taq (Takara) following the manufacturer's instructions. Rice *ACTIN1* served as an internal control to normalize expression levels and the $2^{-\triangle\triangle CT}$ method was used to calculate the relative expression levels with three biological repeats. All of the qPCR primers are listed in Supplementary Table 3.

Promoter activity analysis

A dual-Luc assay was conducted to measure the promoter activity in rice protoplasts, with RENILLA (REN) as an internal control. The approximately 2-kb promoters of $PICI1^{ind}$ and $PICI1^{jap}$ were isolated and cloned into the vector pGreenII 0800-Luc to generate $ProPICI1^{ind}$::Luc and $ProPICI1^{jap}$::Luc constructs. The luciferase activity was calculated by normalizing the REN expression after treatment with 1×10^{-6} M octa-*N*-acetylchitooctaose $(GlcNAc)_8$.

Measurement of Met and ethylene

For Met quantification, approximately 0.1 g of leaves from two-week or one-month-old plants were collected, ground in liquid nitrogen, and resuspended in 1 ml of precooled methanol/acetonitrile/water (2:2:1, v/v/v) buffer, which were then mixed and homogenized by ultrasonication for 30 min. The extract was incubated at −20 °C for 1 h and centrifuged at 4 °C (12,000 rpm for 30 min). The filtered supernatant was collected and analysed on the QTRAP 6500 (AB SCIEX). A Met standard curve is generated to quantify the Met content in each sample.

Ethylene content was determined following a previously reported protocol[11]. In brief, leaves of the same position were detached and cut into 3-cm pieces, and then 3 pieces were put into a 10-ml glass vial with 1 ml distilled water, sealed with a gas-proof septum and left in a growth chamber at 28 °C for 48 h. The gas sample was withdrawn from the air space of each bottle using a gas-tight syringe (Hamilton), and injected into a gas chromatograph (Agilent 6890N) equipped with an activated alumina column and flame ionization detectors for ethylene determination. An ethylene standard curve is generated to quantify ethylene emission in each sample.

LC–MS/MS analysis

To identify PICI1-interacting proteins, total proteins were extracted from leaves of two-week-old seedlings (*PICI1*-GFP/NIL-*Pigm*) after incubation with strain TH12 for 36 h with the IP extraction buffer mentioned above. Non-transgenic NIL-*Pigm* served as a negative control. The PICI1–GFP protein was enriched by immunoprecipitation using anti-GFP antibody, eluted with 0.1 M glycine (pH = 2.5) and the supernatant was used for the mass spectrometric (MS) analysis.

To identify OsMETS1 ubiquitination sites, total proteins were extracted from leaves of two-week-old seedlings (*OsMETS1*-GFP/NIL-*Pigm*) after they were inoculated with TH12 or water as a control for 36 h with IP extraction buffer. The OsMETS1–GFP protein was enriched by immunoprecipitation using anti-GFP antibody, eluted by SDS loading buffer, separated by SDS–PAGE and after staining with Coomassie brilliant blue R-250, the OsMETS1–GFP protein bands were cut out for the mass spectrometric analysis. To identify PICI1 protein modification sites, total proteins were extracted from leaves of two-week-old seedlings (*PICI1*-GFP/NIL-*Pigm*) after they were inoculated with TM21 or water as a control for 36 h with IP extraction buffer. The PICI1–GFP protein was enriched and analysed as mentioned above.

For tandem mass tag (TMT)-based quantitative proteomic analysis, rice leaf sheaths were treated with 1×10^{-6} M octa-*N*-acetylchitooctaose $(GlcNAc)_8$ or water as a control for 10 min. Each group was processed with two independent biological replicates. The concentration of extracted proteins was determined using a bicinchoninic acid (BCA) kit and the proper amount of protein was digested with trypsin using the filter-aided proteome preparation method and then the resulting peptide was processed according to the manufacturer's protocol (Thermo Fisher Scientific). The labelled peptides were fractionated using high pH reverse-phase high pressure liquid chromatography (HPLC), followed by tandem mass spectrometry (MS/MS) in Q Exactive (Thermo Fisher Scientific).

The LC–MS/MS analysis was processed by Applied Protein Technology (Shanghai) as previously described[28]. The entire Rice Annotation Project (RAP) database (http://rapdb.dna.affrc.go.jp/) was searched using Mascot (v.2.3.02, Matrix Science).

Domestication analysis

Nucleotide diversity of *PICI1* and flanking regions was calculated using a sliding window approach. The distribution of nucleotide diversity is plotted in sliding windows of 1 kb with a 100-bp step size. Genetic distance (F_{ST}) between the *japonica* accessions, *indica* accessions and *rufipogon* accessions for the *PICI1* and flanking regions are calculated using a sliding window approach with a 2.5-kb window size and 50-bp step size. The genomic sequences of 27 *japonica* accessions, 19 *indica* accessions and 13 *rufipogon* accessions were acquired from the Rice-PanGenome (http://db.ncgr.ac.cn/RicePanGenome/).

Accession numbers

The sequence data for *PICI1*, *OsMETS1* and *OsMETS2* can be found in the Rice Annotation Project (RAP) database (http://rapdb.dna.affrc.go.jp/) and have been deposited in GenBank: MT920667, MT920668 and MT920669.

Quantification and statistical analysis

No statistical methods were used to predetermine sample size. The experiments were not randomized and the investigators were not blinded to allocation during experiments and outcome assessment. Quantification analyses on lesion areas and protein abundance were conducted by ImageJ software. All values are presented with mean ± s.d. as indicated. Data points are plotted onto the graphs, and the number of samples is indicated in the corresponding figure legends. All statistical analyses were performed by one-way ANOVA followed by Tukey's test with GraphPad software or by two-sided Student's *t*-test with Microsoft Excel software. Detailed information about statistical analysis values for all experiments is provided in Supplementary Table 4.

Reporting summary

Further information on research design is available in the Nature Research Reporting Summary linked to this paper.

Data availability

All data are available within this Article and its Supplementary Information. Original gel blots are shown in Supplementary Fig. 1. Original data points in graphs are shown in the Source Data files. Statistical analyses of this study are provided in Supplementary Table 4. The sequences of PICI1, OsMETS1 and OsMETS2 have been deposited and made publicly available in GenBank with accession codes MT920667, MT920668 and MT920669, respectively. Protein structure models of Protein Data Bank (PDB) ID 2WP7 and PDB ID 1U1U were obtained from the PDB. Source data are provided with this paper.

39. He, J. et al. A LysM receptor heteromer mediates perception of arbuscular mycorrhizal symbiotic signal in rice. *Mol. Plant* **12**, 1561–1576 (2019).
40. Ma, X. et al. A robust CRISPR/Cas9 system for convenient, high-efficiency multiplex genome editing in monocot and dicot Plants. *Mol. Plant* **8**, 1274–1284 (2015).
41. Zhai, K. et al. RRM transcription factors interact with NLRs and regulate broad-spectrum blast resistance in rice. *Mol. Cell* **74**, 996–1009 (2019).
42. Park, C.-H. et al. The *Magnaporthe oryzae* effector AvrPiz-t targets the RING E3 ubiquitin ligase APIP6 to suppress pathogen-associated molecular pattern-triggered immunity in rice. *Plant Cell* **24**, 4748–4762 (2012).

Acknowledgements We thank J. Zhou and J. Li for critical reading and discussion; X. Wei and G. Zhang for providing the rice germplasm and CSSL; J. Zhang for help with ethylene measurement; S. Wang for help with Met measurement; B. Liu, C. Wang and Z. Gu for help with bioinformatic analysis; and X. Fu for sharing HA-Ub plasmids. This work was supported by grants from the National Natural Science Foundation of China (32088102, 31720103913 and U20A2021), the Chinese Academy of Sciences (XDB27040201 and XDA24010304), the National Key Research and Development Program of China (2016YFD0100600), the Science and Technology Commission of Shanghai Municipality (19391900300), the Project of Special Funding for Crop Science Discipline Development of Yangzhou University (yzuxk202006) and the National Key Laboratory of Plant Molecular Genetics. K.Z. was supported by the National Postdoctoral Program for Innovative Talents (BX20190346) and by the Shanghai Postdoctoral Excellence Program.

Author contributions K.Z. and Z.H. conceived and designed the experiments. K.Z. and D.L. performed most experiments, including the Y2H, SLC, BiFC, co-IP, subcellular localization, cell-free degradation assay, deubiquitination assay, ROS detection and western blots. K.Z., H.L. and Y.W. performed Met and ethylene measurement. K.Z., H.L. and F.J. performed RNA analysis. K.Z., D.L., B.Y. and X.G. performed pathoassays. D.L. and H.L. performed agronomic traits analysis. K.Z., J.L., Z.L., L.H., X.W. and J.-Y.L. generated material used in this study. J.M. performed the domestication analysis. H.G. and B.H. supervised Y.W. and J.M., respectively. L.Z., E.W., Y.D., C.-K.W., H.G. and B.H. provided theoretical contributions to the project. K.Z., D.L. and Z.H. analysed the data and wrote the paper.

Competing interests The authors declare no competing interests.

Additional information
Supplementary information The online version contains supplementary material available at https://doi.org/10.1038/s41586-021-04219-2.

Correspondence and requests for materials should be addressed to Zuhua He.

Peer review information *Nature* thanks Nicholas Talbot and the other, anonymous, reviewer(s) for their contribution to the peer review of this work.

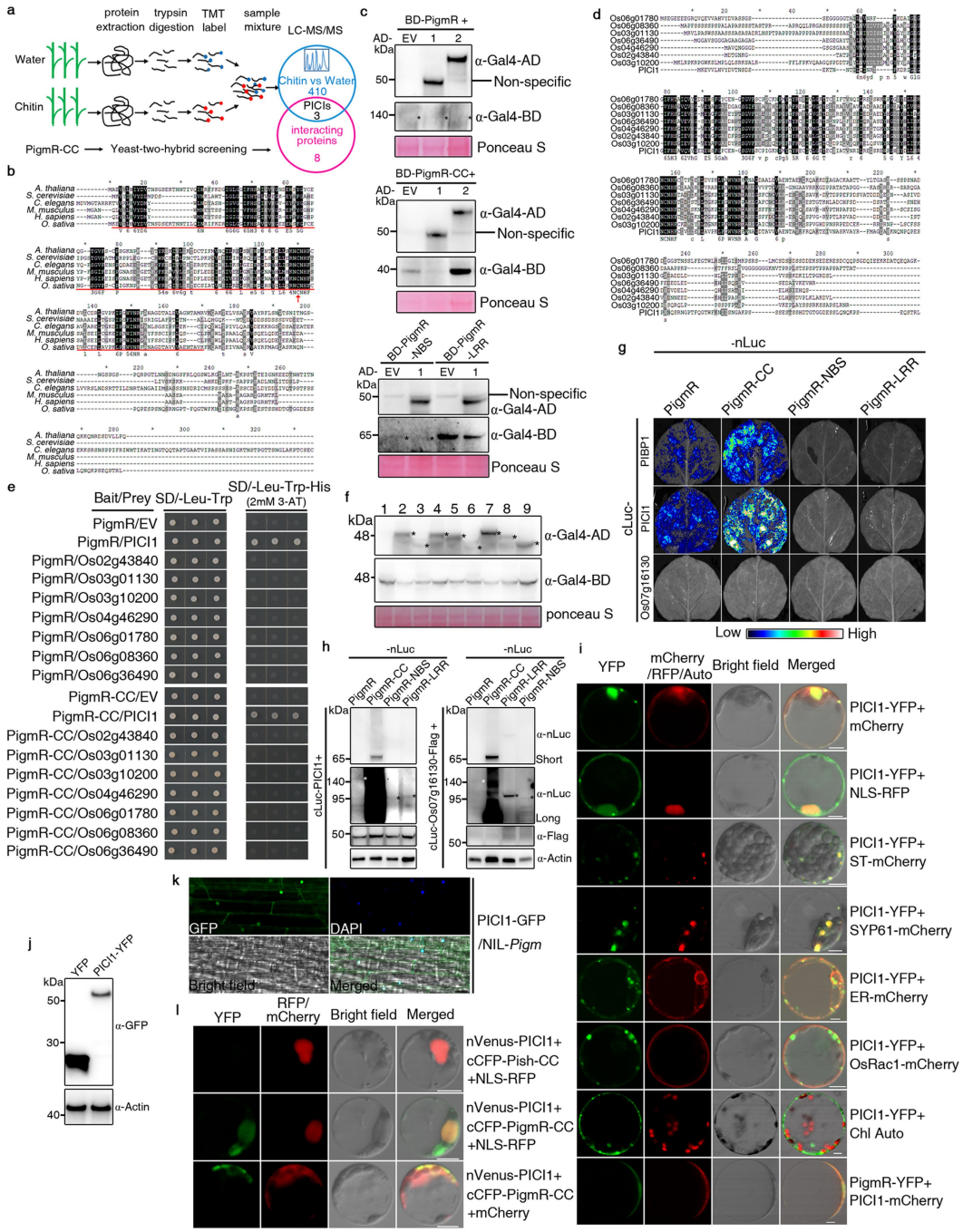

Extended Data Fig. 1 | See next page for caption.

Extended Data Fig. 1 | Screening of PICIs and PigmR–PICI1 interaction analysis. a, The workflow for identifying the proteins involved in both PTI and ETI. Tandem Mass Tag (TMT)-based proteomic analysis was performed to investigate the global changes of rice protein profiling with chitin treatment, the blue circle denotes the chitin-induced 413 candidate proteins. Total 11 PigmR-CC interacting proteins were identified through yeast-two-hybrid screen and shown with the pink circle. The overlap between the blue and pink circles indicates 3 PICI candidates. **b**, Protein alignment of PICI1 and its homologs in *A. thaliana*, *S. cerevisiae*, *C. elegans*, *M. musculus* and *H. sapiens* (NP_194296.1, NP_594707.2, NP_741592.1, NP_077244.1 and NP_057160.2, respectively) with MegAlign software. The conserved PPPDE region is underlined in red and the conserved site Cys115 residue is marked with red arrow. **c**, Immunodetection of protein expression in yeast. pDEST22 (EV), pDEST22-PICI1 (1) and pDEST22-Os07g16130 (2) detected using anti-GAL4-AD antibody. pDEST32-PigmR (BD-PigmR), pDEST32-PigmR-CC (BD-PigmR-CC), pDEST32-PigmR-NBS (BD-NBS) and pDEST32-PigmR-LRR (BD-LRR) detected using anti-GAL4-BD antibody. The asterisks indicate the target proteins. **d**, Protein alignment of PICI1 and its homologs in rice. **e**, PigmR and PigmR-CC specifically interact with PICI1 but not its homologs in Y2H assay. **f**, Immunodetection of protein levels in yeast. Upper panel (AD), pDEST22 (lane 1), pDEST22-PICI1 (lane 2), -Os02g43840 (lane 3), -Os03g01130 (lane 4), -Os03g10200 (lane 5), -Os04g46290 (lane 6), -Os06g01780 (lane 7), -Os06g08360 (lane 8), -Os06g36490 (lane 9), detected using anti-GAL4-AD antibody; middle panel (BD), pDEST32-PigmR-CC, detected using anti-GAL4-BD antibody. The asterisks indicate the target proteins. **g**, SLC assay of PigmR-PICI1 interaction in *N. benthamiana*. PIBP1 and Os07g16130 served as positive and negative control, respectively. Fluorescence signal intensity is indicated. **h**, Western blot confirming expression of proteins in *N. benthamiana*. Note that cLuc-PICI1 was detected using anti-PICI1 antibody. Short, long = short or long exposure. **i**, PICI1-YFP was co-expressed with various known organelle markers as indicated in rice protoplasts. mCherry = cytoplasmic marker, NLS-RFP = nucleus marker, ST-mCherrry = trans-Golgi cisternae marker, SYP61-mCherry = trans-Golgi network/early endosome (TGN/EE) marker, ER-mCherry = endoplasmic reticulum marker, OsRac1-mCherrry = cell member marker, Chl Auto = Chloroplast autofluorescence. **j**, Western blot confirming expression of PICI1-YFP without free YFP in rice protoplast. **k**, Localization of PICI1-GFP in representative root cells of stable transgenic plants. DAPI staining indicates the nucleus. **l**, Bimolecular fluorescence complementation (BiFC) verifies the PigmR-CC/PICI1 interaction in rice protoplasts. Pish-CC served as a negative control. Ponceau S staining (**c**, **f**) or Actin (**h**, **j**) served as loading control. Scale bars, 5 μm (**i**, **l**) or 10 μm (**k**). Experiments were repeated twice (**c**, **f**, **h**) or three times with similar results (**e**, **g**, **i**–**l**).

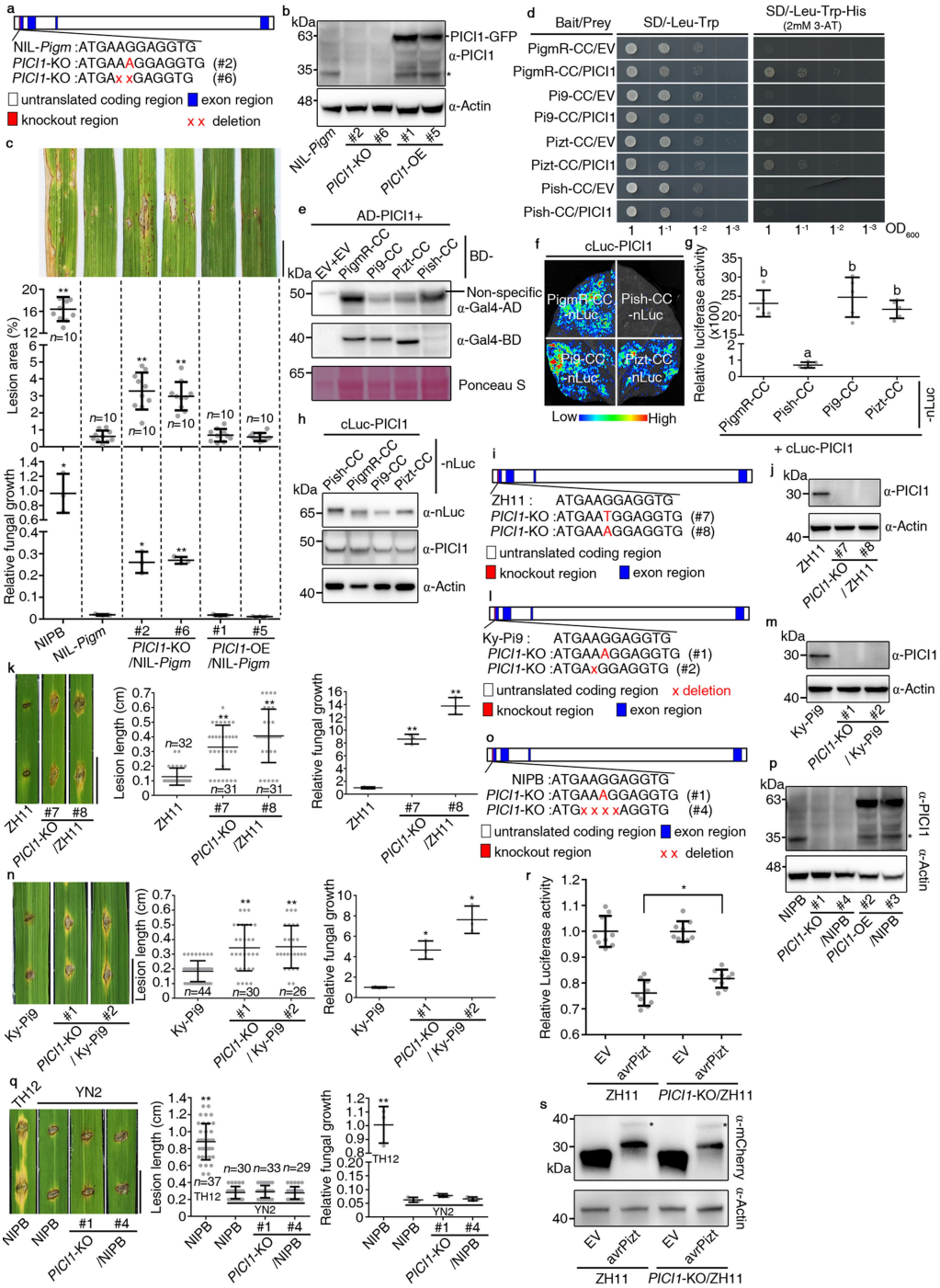

Extended Data Fig. 2 | See next page for caption.

Extended Data Fig. 2 | PICI1 is involved in PigmR-, Pizt- and Pi9- but not Pish-mediated blast resistance. a, **i**, **l**, **o**, Schematic of two independent *PICI1* knockout lines in NIL-*Pigm* (**a**), ZH11 (*Pizt*-containing) (**i**), Ky-*Pi9* (*Pi9*-containing) (**l**) and NIPB (*Pish*-containing) (**o**), respectively. **b**, **j**, **m**, **p**, Protein analysis of PICI1 in the corresponding transgenic plants using an anti-PICI1 antibody. The asterisk indicates the endogenous PICI1 and the band around 63 kDa indicates the PICI1-GFP fusion protein (**b**, **p**). **c**, Blast resistance of NIL-*Pigm*, *PICI1*-KO/NIL-*Pigm* and *PICI1*-OE/NIL-*Pigm* lines at 7dpi with punch injection inoculation (TH12). NIPB served as a susceptible control. **d**, Y2H assay of interactions between PICI1 and the CC domains of PigmR, Pi9, Pizt and Pish. EV, empty vector. **e**, Immunodetection of protein levels in yeast. Upper panel (AD), pDEST22-PICI1, detected using anti-GAL4-AD antibody; middle panel (BD), PigmR-CC, Pi9-CC, Pizt-CC and Pish-CC, detected using anti-GAL4-BD antibody. **f**, SLC confirmation of the PICI1-Pizt-CC and PICI1/Pi9-CC interactions in *N. benthamiana*. PigmR-CC and Pish-CC served as positive and negative control, respectively. Fluorescence signal intensity is indicated. **g**, Relative luciferase activity of protein-protein interactions was measured. One-way ANOVA with Tukey's test (mean ± s.d.; $n = 5$, biologically independent samples). Different letters indicate significant difference at $P < 0.05$. **h**, Western blot analysis confirming the expression level of each protein in *N. benthamiana*. **k**, **n**, **q**, Punch inoculation of *PICI1*-KO transgenic plants in ZH11 (**k**), Ky-*Pi9* (**n**) and NIPB (**q**). Blast resistance of WT and two representative transgenic lines, 5 dpi with avirulent strain YN2 (**k**, **q**) or Guy11 (**n**). TH12 served as a susceptible control (**q**). **r**, Transient assay of cell death in rice protoplast. Relative luciferase activity was measured after transformation with avrPizt-mCherry in rice protoplasts derived from ZH11 or *PICI1*-KO/ZH11. Empty vector (EV) was used as a negative control. Two-tailed Student's *t*-test (mean ± s.d.; $n = 9$, biologically independent samples). **s**, Western blot analysis confirming expression of proteins in rice protoplasts. Actin (**b**, **h**, **j**, **m**, **p**, **s**) or Ponceau S staining (**e**) served as loading control. The asterisks indicate the target proteins. For **c**, **k**, **n**, **q**, data were analysed by two-tailed Student's *t*-test. Fungal growth (mean ± s.d.; $n = 3$, biologically independent samples), lesion lengths or areas (mean ± s.d.; n = numbers of biologically independent samples in the graphs). Scale bars, 1 cm. Asterisks represent significant difference ($^*P < 0.05$, $^{**}P < 0.01$) (**c**, **k**, **n**, **q**, **r**). Exact *P* values are provided in Supplementary Table 4 (**c**, **g**, **k**, **n**, **q**, **r**). Experiments were repeated twice (**b**, **e**, **h**, **j**, **m**, **p**) or three times with similar results (**c**, **d**, **f**, **g**, **k**, **n**, **q**, **r**, **s**).

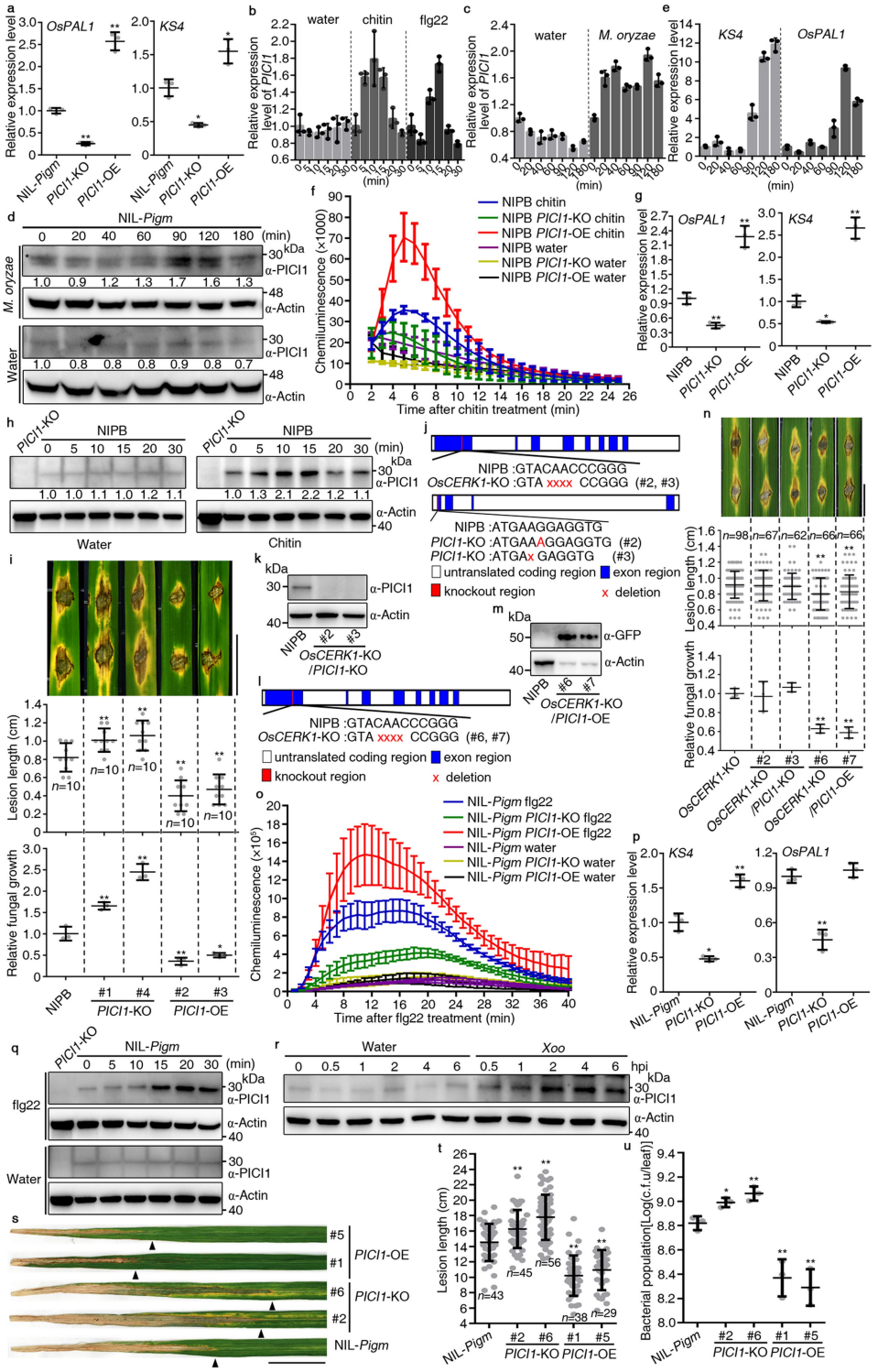

Extended Data Fig. 3 | See next page for caption.

Extended Data Fig. 3 | PICI1 is involved in chitin- and flg22-induced PTI responses. a, **g**, **p**, Induction of the PTI-related defence genes Os*PAL1* and *KS4* at 1 h after chitin (**a**, **g**) or flg22 (**p**) incubation in WT, *PICI1*-KO and *PICI1*-OE lines in NIL-*Pigm* (**a**, **p**) or NIPB (**g**) background. Two-tailed Student's *t*-test (mean ± s.d.; $n = 3$, biologically independent samples). **b**, **c**, Induction of *PICI1* in NIL-*Pigm* upon chitin/flg22 treatment (**b**) and during *M. oryzae*TM21 infection (**c**) with water as control. **d**, **h**, PICI1 was induced upon *M. oryzae* TM21 infection (**d**) and chitin treatment (**h**) with water as control. The asterisk indicates endogenous PICI1 (**d**). The relative PICI1 protein abundance was indicated. **e**, Induction of PTI-related defence genes *KS4* and *OsPAL1* in NIL-*Pigm* leaves during *M. oryzae* TM21 infection. **f**, **o**, Chitin- (**f**) or flg22- (**o**) induced ROS burst in WT, *PICI1*-KO and *PICI1*-OE lines in NIPB (**f**) or NIL-*Pigm* (**o**) background. Data are mean ± s.d. ($n = 9$, biologically independent samples). **i**, Disease resistance of *PICI1* transgenic plants in NIPB. **j**, **l**, Schematic of two independent *PICI1*/*OsCERK1* double knockout (**j**) and *PICI1*-OE/*OsCERK1*-KO (**l**) lines in NIPB. **k**, **m**, Protein levels of PICI1 (**k**) or PICI1-GFP (**m**) in *PICI1*/*OsCERK1*-KO (**k**) or *PICI1*-OE/*OsCERK1*-KO (**m**). **n**, Punch inoculation of *OsCERK1*-KO, *PICI1*/*OsCERK1*-KO and *PICI1*-OE/*OsCERK1*-KO transgenic lines. **q**, **r**, PICI1 was induced upon flg22 treatment (**q**) and bacterial *Xoo* (strain, PXO99^{A}) infection (**r**) with water as control. **s**–**u**, Disease resistance to bacterial *Xoo* in the *PICI1* transgenic lines in NIL-*Pigm*. Triangles represent the end of bacterial infection sites. For **i**, **n**, **t**, **u**, data were analysed by two-tailed Student's *t*-test. Lesion lengths (mean ± s.d.; n = numbers of biologically independent samples in the graphs), fungal or bacterial growth (mean ± s.d.; $n = 3$, biologically independent samples). For **b**, **c**, **e**, data are mean ± s.d. ($n = 3$, biologically independent samples). The rice *ACTIN1* served as an internal control (**a**-**c**, **e**, **g**, **p**). Actin was detected as a loading control (**d**, **h**, **k**, **m**, **q**, **r**). Blast resistance of representative transgenic lines, 5 dpi with virulent strain TH12 (**i**, **n**). Scale bars, 1 cm (**i**, **n**) or 5 cm (**s**). Asterisks represent significant difference ($^{*}P < 0.05$, $^{**}P < 0.01$) (**a**, **g**, **i**, **n**, **p**, **t**, **u**). Experiments were repeated twice (**k**, **m**) or three times with similar results (**a**–**i**, **n**, **o**–**u**).

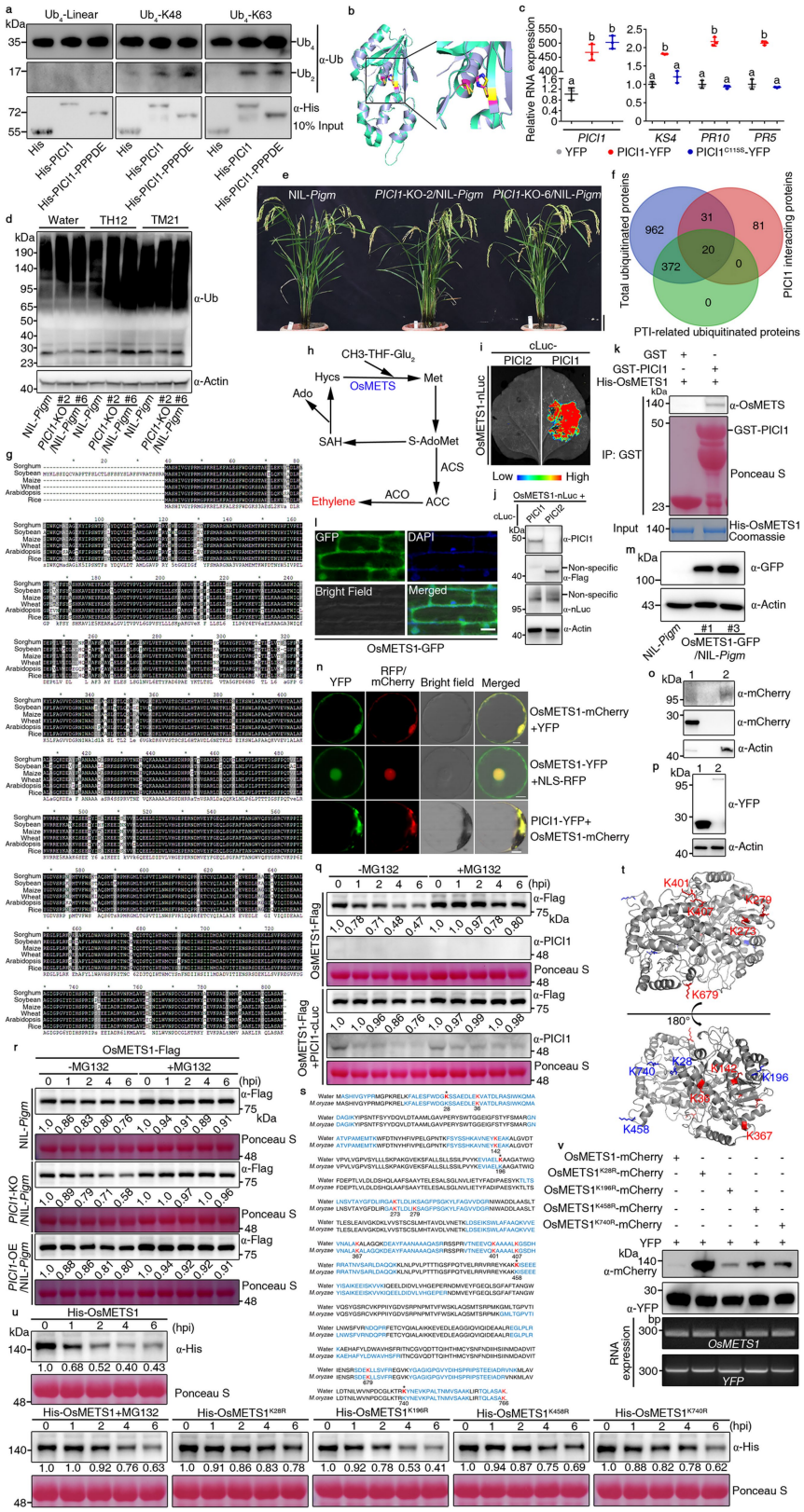

Extended Data Fig. 4 | See next page for caption.

Extended Data Fig. 4 | PICI1 functions as a deubiquitinase, and interacts with and stabilizes OsMETS1. a, His-PICI1 and His-PICI1-PPPDE displayed cleavage activity toward K48- and K63-linked but not linear ubiquitin in vitro. His alone served as a control. **b**, Homology model of PICI1-PPPDE domain (cyan) aligned with Desi-1 (PDB ID code 2WP7) (blue) using PyMOL. The putative catalytic dyad residues of H41 and C115 in PICI1 are shown in yellow and the catalytic residues of Desi-1 H38 and C108 are shown in magenta. The boxed section is magnified for close view. **c**, Induction of *KS4*, *PR10* and *PR5* in PICI1-YFP or PICI1^{C115S}-YFP overexpression protoplast after chitin treatment (1 hpi) with the empty vector control. Lowercase letters indicate statistical significance ($P < 0.05$). One-way ANOVA with Tukey's test. Data are mean ± s.d. ($n = 3$, biologically independent samples). Exact *P* values are provided in Supplementary Table 4. **d**, Ubiquitin conjugation in total protein extracts from 2-week-old NIL-*Pigm* and *PICI1*-KO/NIL-*Pigm*, after spraying TH12 or TM21 with water as control for 36 h. **e**, Morphological phenotype of mature plants of wild-type and *PICI1*-KO/NIL-*Pigm*. No obvious change in morphology was observed in the *PICI1*-KO plants. Scale bar, 10 cm. **f**, Venn diagram showing the number of total ubiquitinated proteins (blue), PICI1 interacting candidates identified in IP–MS (red), PTI-related ubiquitinated proteins (green) and overlapping proteins. **g**, Protein alignment of OsMETS1 and its homologs in sorghum, soybean, maize, wheat and Arabidopsis (XP_021301657.1, XP_003542326.1, PWZ52049.1, TraesCS4D02G012900.2 and XP_002871787.1) with MegAlign software. **h**, Ethylene biosynthesis pathway in plants. S-AdoMet, S-adenosylmethionine; Hcys, homocysteine; THF, tetrahydrofolate; SAH, S-adenosylhomocysteine; Ado, adenosine; ACS, 1-aminocyclopropane-1-carboxylate synthase; ACC, 1-aminocyclopropane-1-carboxylate. **i**, A SLC assay of OsMETS1 and PICI1 interaction in *N. benthamiana*. PICI2 served as a negative control. Fluorescence signal intensity is indicated. **j**, Western blot confirming protein expression in *N. benthamiana*. **k**, GST-PICI1 pulls down His-OsMETS1 in vitro. **l**, Subcellular localization of OsMETS1-GFP in OsMETS1-GFP/NIL-*Pigm* root. DAPI staining indicates the nucleus. Scale bars, 10 μm. **m**, Immunodetection of OsMETS1-GFP in transgenic lines, with NIL-*Pigm* as a negative control. **n**, Subcellular localization of OsMETS1 and co-localization of PICI1-YFP/OsMETS1-mCherry in rice protoplasts. Scale bars, 5 μm. **o**, Western blot confirming expression of OsMETS1-mCherry without free mCherry in rice protoplast. mCherry (lane 1), OsMETS1-mCherry (lane 2). **p**, Western blot confirming expression of OsMETS1-YFP without free YFP in rice protoplast. YFP (lane 1), OsMETS1-YFP (lane 2). **q**, Degradation of OsMETS1-Flag was proteasome-dependent and delayed by PICI1 in cell-free system. **r**, PICI1 stabilizes OsMETS1-Flag in rice plants. The lysates from WT, *PICI1*-KO and *PICI1*-OE plants were co-incubated with OsMETS1-Flag in the presence or absence of MG132. **s**, Peptide coverage and ubiquitination sites identified in OsMETS1 by tandem mass spectrometry after *M. oryzae* (TH12) or water treatment for 36 h. The various peptides identified by mass spectrometry are shown in blue; the lysine acceptor sites detected in red are numbered below with positions; the four specific deubiquitination sites are denoted with asterisks. **t**, Structure model for OsMETS1. Homology model of the OsMETS1 based on the crystal structure of Arabidopsis Met synthase (PDB ID code 1U1U) and analysed by PyMOL. The four lysines identified as deubiquitination sites were shown in blue. The other lysine acceptor sites were shown in red. **u**, Cell-free degradation assays show the proteasome-dependent degradation of His-OsMETS1 and delayed degradation of His-OsMETS1 mutant variants. Purified recombinant His-OsMETS1 and its mutants were incubated with protein extracts from non-infected NIPB. His alone served as a negative control. **v**, The OsMETS1 mutants showed higher protein accumulation compared to wild-type OsMETS1 in protoplasts. The YFP tag protein was expressed as an internal control. The transcript levels were determined by semi-quantitative PCR. Actin was detected as a loading control (**d**, **j**, **m**, **o**, **p**). Ponceau S staining served as loading control (**q**, **r**, **u**). The protein abundance was quantified using ImageJ and indicated under lanes (**q**, **r**, **u**). Experiments were repeated twice (**j**, **m**, **o**, **p**) or three times with similar results (**a**, **c**, **d**, **i**, **k**, **l**, **n**, **q**, **r**, **u**, **v**).

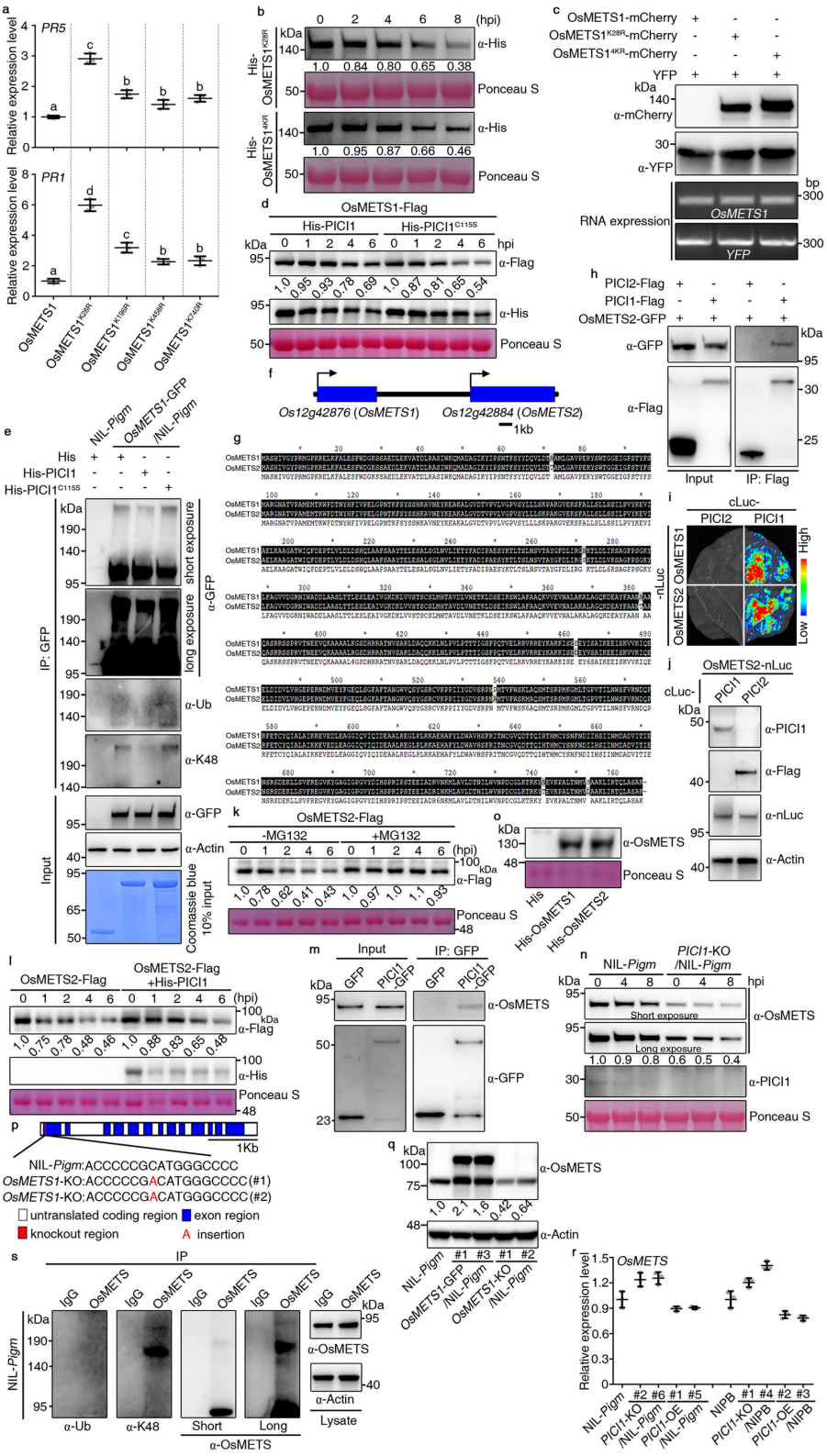

Extended Data Fig. 5 | See next page for caption.

Extended Data Fig. 5 | PICI1 directly deubiquitinates and stabilizes OsMETS. **a**, Induction of *PR5* and *PR1* in OsMETS1, OsMETS1^{K28R}, OsMETS1^{K196R}, OsMETS1^{K458R} and OsMETS1^{K740R} overexpression protoplasts after chitin treatment (1 hpi). Lowercase letters indicate statistical significance ($P < 0.05$). One-way ANOVA with Tukey's test. Data are mean ± s.d. ($n = 3$, biologically independent samples). Exact *P* values are provided in Supplementary Table 4. **b**, Cell-free degradation assays show the delayed degradation of His-OsMETS1^{4KR} mutant variant, compared to His-OsMETS1^{K28R}. Purified recombinant fusion proteins were incubated with non-infected NIPB extracts. **c**, The OsMETS1^{4KR} mutant showed higher protein accumulation compared to wild-type OsMETS1 and OsMETS1^{K28R} in protoplasts. The YFP tag protein was expressed as an internal control. The transcript levels were determined by semi-quantitative PCR. **d**, Stability of the OsMETS1-Flag depends on His-PICI1 but not the His-PICI1^{C115S} in cell-free degradation assay. **e**, Deubiquitination analysis of ubiquitin-modified OsMETS1-GFP, immunoprecipitated from *OsMETS1*-GFP/NIL-*Pigm* plants, by incubating with recombinant His-PICI1 or His-PICI1^{C115S} respectively. **f**, Tail-to-head organization of *OsMETS1* and *OsMETS2* genes in rice. **g**, Protein alignment of OsMETS1 and OsMETS2 with MegAlign software. **h**, Co-IP assay of PICI1 with OsMETS2 in rice. PICI2 served as a negative control. **i**, A SLC assay showed that both OsMETS1 and OsMETS2 interacted with PICI1 in *N. benthamiana*. PICI2 was used as a negative control. Fluorescence signal intensity is indicated. **j**, Western blot confirming protein expression in *N. benthamiana*. **k**, Cell-free degradation assay showed the proteasome-dependent degradation of OsMETS2-Flag in *N. benthamiana*. **l**, Cell-free degradation assay showed the delayed degradation of OsMETS2 in presence of recombinant His-PICI1. **m**, Co-IP assay of PICI1 with endogenous OsMETS in rice. The GFP negative control and PICI1-GFP were constitutively expressed in transgenic rice plants. anti-OsMETS, recognizing both OsMETS1 and OsMETS2. **n**, Cell-free degradation assay showed that endogenous OsMETS degradation was delayed by PICI1. **o**, Immunodetection of the recombinant His-OsMETS1 and His-OsMETS2 using the anti-OsMETS antibody. His alone served as a negative control. **p**, A schematic diagram of two independent *OsMETS1*-KO lines in NIL-*Pigm* background. **q**, Protein levels of OsMETS in NIL-*Pigm*, *OsMETS1*-GFP/NIL-*Pigm* and *OsMETS1*-KO/NIL-*Pigm* plants using the anti-OsMETS antibody. The band around 75 kDa indicates the endogenous OsMETS. **r**, Relative transcript levels of *OsMETS* in the wild-type, *PICI1*-KO and *PICI1*-OE lines in NIL-*Pigm* and NIPB background. Data are mean ± s.d. ($n = 3$, biologically independent samples). **s**, Analysis of endogenous OsMETS ubiquitination. OsMETS was immunoprecipitated from wild-type NIL-*Pigm* with anti-OsMETS or anti-IgG as negative control. Short, long = Short or long exposure. The protein abundance was quantified using ImageJ and indicated under lanes (**b**, **d**, **k**, **l**, **n**, **q**). Ponceau S staining (**b**, **d**, **k**, **l**, **n**, **o**) or Actin (**e**, **j**, **q**, **s**) was used as a control for equal loading. The rice *ACTIN1* served as an internal control (**a**, **r**). Experiments were repeated twice (**h**, **j**, **m**, **n**, **o**, **s**) or three times (**a**–**e**, **i**, **k**, **l**, **q**, **r**) with similar results.

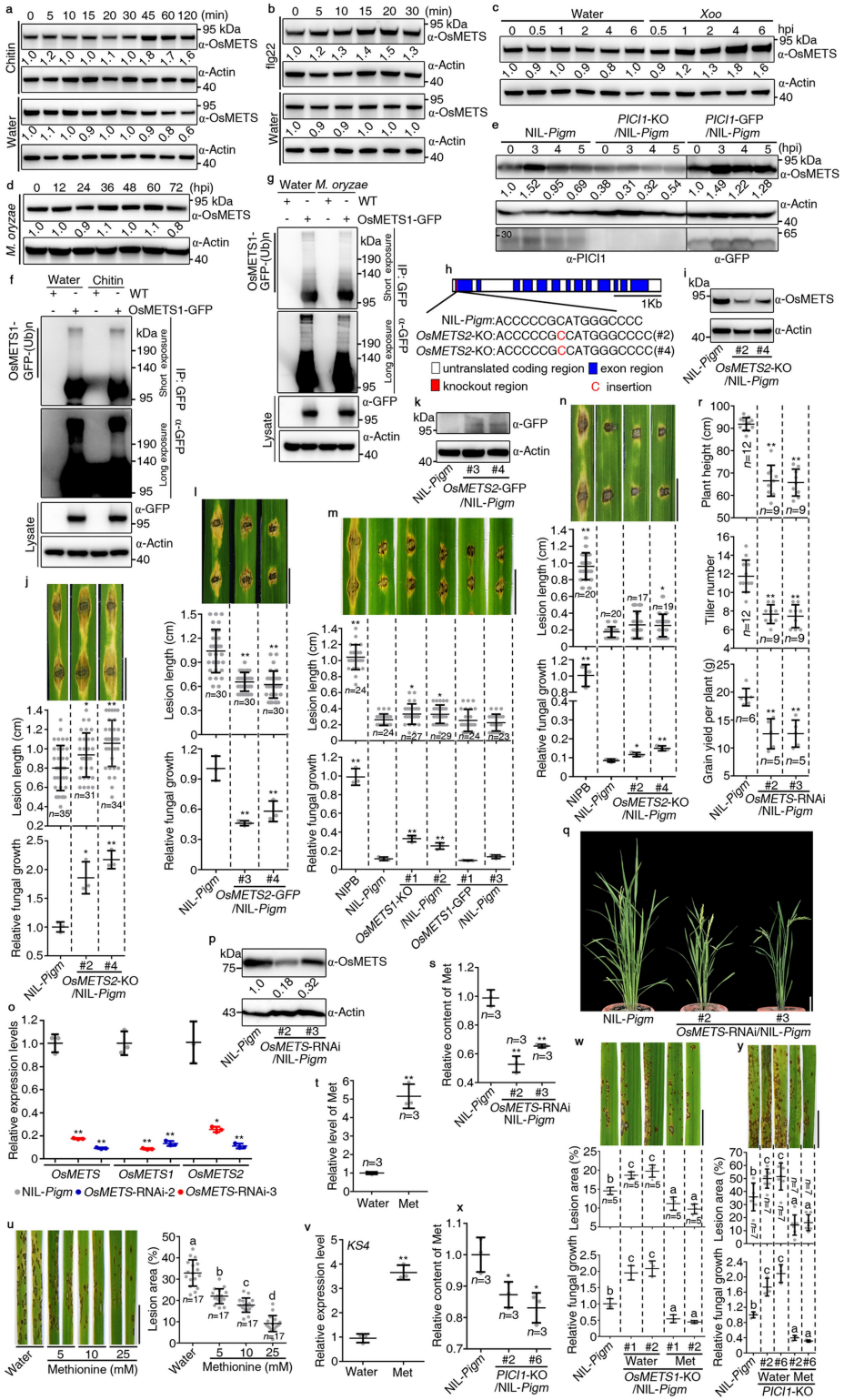

Extended Data Fig. 6 | See next page for caption.

Extended Data Fig. 6 | OsMETS functions in rice PTI and ETI. **a**, **b**, **c**, **d**, OsMETS is induced upon treatment of chitin (**a**) or flg22 (**b**), and infection of *Xoo* (PXO99^{A}) (**c**) or *M. oryzae* (TM21) (**d**). **e**, Protein accumulation of OsMETS in NIL-*Pigm*, *PICI1*-KO/NIL-*Pigm* and *PICI1*-GFP/NIL-*Pigm* in early infection stage (TM21). **f**, **g**, Decreased ubiquitination of OsMETS1-GFP in PTI (**f**) and ETI (**g**). The protein extracts from OsMETS1-GFP/NIL-*Pigm* plants incubated with chitin for 1h (**f**) or infected with TH12 for 36 h (**g**), with water as control, was analysed. NIL-*Pigm* served as a negative control. **h**, A schematic diagram of two independent *OsMETS2*-KO lines in NIL-*Pigm*. **i**, Decreased protein levels of OsMETS in *OsMETS2*-KO/NIL-*Pigm* compared with NIL-*Pigm*. **j**, **l**, Basal blast resistance of NIL-*Pigm*, *OsMETS2*-KO/NIL-*Pigm* (**j**) and *OsMETS2*-GFP/NIL-*Pigm* (**l**) at 5 dpi with punch inoculation (TM21). **k**, Immunodetection of the OsMETS2-GFP in the two independent transgenic lines, with NIL-*Pigm* as a negative control. **m**, **n**, Disease resistance of WT, *OsMETS1*-KO (**m**), *OsMETS1*-OE (**m**) and *OsMETS2*-KO (**n**) were shown, 5 dpi with TH12, NIPB served as a susceptible control. **o**, Relative transcript levels of *OsMETS1*, *OsMETS2* and *OsMETS* in NIL-*Pigm* and two *OsMETS*-RNAi lines. **p**, Protein levels of OsMETS in NIL-*Pigm* and *OsMETS*-RNAi lines. **q**, Morphological phenotype of NIL-*Pigm* and *OsMETS*-RNAi/NIL-*Pigm* lines at mature stage in the paddy field. **r**, *OsMETS*-RNAi/NIL-*Pigm* plants significantly reduced plant height (upper panel), tiller number (middle panel), grain yield per plant (lower panel). **s**, Relative Met contents in WT and *OsMETS*-RNAi/NIL-*Pigm*. **t**, Increased Met accumulation in NIL-*Pigm* seedling shoots after root incubation with 25 mM Met for 48 h. **u**, Increased blast resistance after Met treatment in NIPB. **v**, Induction of the defence gene *KS4* at 48 h after root dipping with 25 mM Met solution or water in NIL-*Pigm*. **w**, **y**, Basal blast resistance of Met-treated *OsMETS1*-KO/NIL-*Pigm* at 5 dpi (**w**) or *PICI1*-KO/NIL-*Pigm* at 7 dpi (**y**). Met solution (10 mM) or water was supplied from the roots for 48 h and plants were then inoculated with TM21. **x**, Relative Met contents in WT and *PICI1*-KO/NIL-*Pigm* lines. For **j**, **l**, **m**, **n**, data were analysed by two-tailed Student's *t*-test. Lesion lengths (mean ± s.d.; *n* = numbers of biologically independent samples in the graphs), fungal growth (mean ± s.d.; *n* = 3, biologically independent samples). For **u**, **w**, **y**, one-way ANOVA with Tukey's test. Lesion areas (mean ± s.d.; *n* = numbers of biologically independent samples in the graphs), fungal growth (mean ± s.d.; *n* = 3, biologically independent samples). Lowercase letters indicate statistical significance ($P < 0.05$). For **r**, **s**, **t**, **x**, data were analysed by two-tailed Student's *t*-test (mean ± s.d.; *n* = numbers of biologically independent samples in the graphs). In **o**, **v**, two-tailed Student's *t*-test (mean ± s.d.; *n* = 3, biologically independent samples). Asterisks indicate significant differences ($^{*}P < 0.05$, $^{**}P < 0.01$) (**j**, **l**-**o**, **r**–**t**, **v**, **x**). Exact *P* values are provided in Supplementary Table 4 (**j**, **l**–**o**, **r**–**y**). Scale bars, 1 cm (**j**, **l**–**n**, **u**, **w**, **y**), 10 cm (**q**). Relative protein abundance was indicated below (**a**–**e**, **p**). Actin was detected as a loading control (**a**–**g**, **i**, **k**, **p**). The rice *ACTIN1* served as an internal control (**o**, **v**). Experiments were independently repeated twice (**i**, **k**, **p**, **r**) or three times (**a**–**g**, **j**, **l**–**o**, **s**–**y**) with similar results.

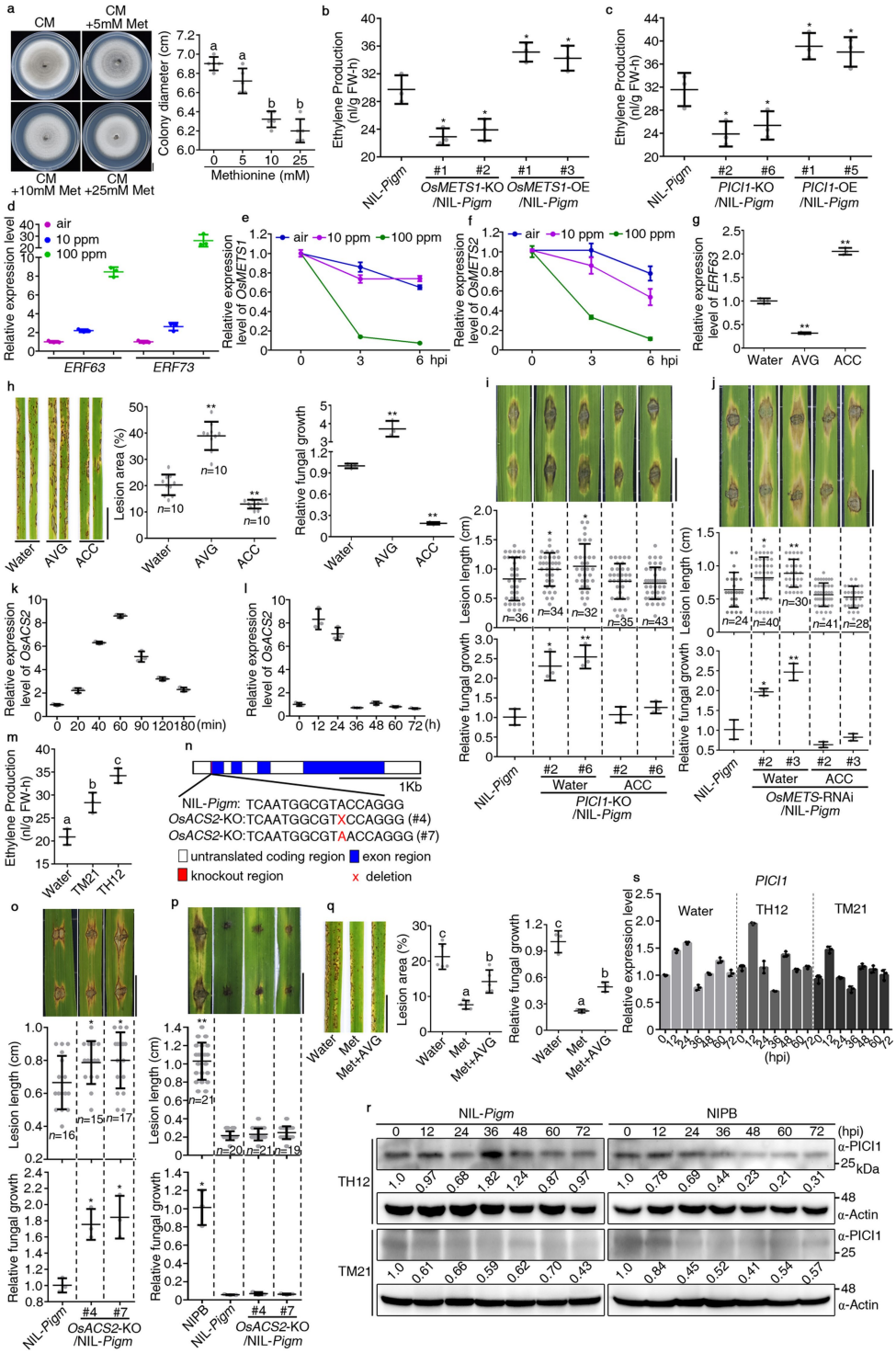

Extended Data Fig. 7 | See next page for caption.

Extended Data Fig. 7 | PICI1–OsMETS module confers blast resistance through regulating Met–ethylene biosynthesis. a, High Met concentrations (10 and 25 mM) inhibit blast fungal growth on medium. The *M. oryzae* isolate TH12 was inoculated on the complete medium (CM) with Met supplement. The colony diameters were measured. One-way ANOVA with Tukey's test (mean ± s.d.; $n = 5$, biologically independent samples). **b**, **c**, Ethylene contents in WT and transgenic lines of *OsMETS1* (*OsMETS1*-KO and *OsMETS1*-OE) (**b**) and *PICI1* (*PICI1*-KO and *PICI1*-OE) (**c**) infected by TM21 (2-week-old, 36 hpi). Two-tailed Student's *t*-test (mean ± s.d.; $n = 3$, biologically independent experiments). **d**, Induction of *ERF63* and *ERF73* by ethylene treatment in NIL-*Pigm*. Two-week-old seedlings were placed into sealed containers with 10 or 100 ppm (μl/L) ethylene, or air as control for 3 h to analyse gene expression. **e**, **f**, Suppression of *OsMETS1* (**e**) and *OsMETS2* (**f**) expression by ethylene treatment (100 ppm) in NIL-*Pigm*. **g**, Relative expression of *ERF63* at 1 d treatment with 10 μM AVG or 20 μM ACC or water. *ERF63* was chosen as a marker gene for AVG and ACC responses. Two-tailed Student's *t*-test (mean ± s.d.; $n = 3$, biologically independent samples). **h**, Effects of AVG and ACC on basal blast resistance in NIPB. Two-week-old seedlings were pre-treated with 10 μM AVG, or 20 μM ACC or water for 1 d and then spray-inoculated with rice blast (TH12), 5 dpi. **i**, **j**, Basal blast resistance of ACC-treated *PICI1*-KO/NIL-*Pigm* (**i**) and *OsMETS*-RNAi/NIL-*Pigm* (**j**) plants. ACC solution (20 μM) or water was supplied from the leaves and inoculated with TM21, 5 dpi. **k**, **l**, Induction of *OsACS2* in NIL-*Pigm* leaves at early stage by TM21 (**k**, PTI) or late stage by TH12 (**l**, ETI) infection. **m**, Enhanced ethylene production in NIL-*Pigm* after rice blast infection (TH12 or TM21), with water as a control for 36 h. One-way ANOVA with Tukey's test (mean ± s.d.; $n = 3$, biologically independent experiments). **n**, A schematic diagram of *OsACS2*-KO lines in NIL-*Pigm*. **o**, Basal blast resistance in NIL-*Pigm* and *OsACS2*-KO/NIL-*Pigm*, at 5 dpi with punch inoculation (TM21). **p**, Disease resistance of wild type and *OsACS2*-KO lines were shown, 5 dpi with TH12, NIPB served as a susceptible control. **q**, Met enhances rice blast resistance via ethylene biosynthesis. A Met solution (10 mM) or water was supplied from NIL-*Pigm* roots for 48 h and pre-treated with 10 μM AVG for 36 h before spray inoculation with rice blast (TM21). One-way ANOVA with Tukey's test. Lesion areas (mean ± s.d.; $n = 5$, biologically independent samples), fungal growth (mean ± s.d.; $n = 3$, biologically independent samples). **r**, Protein levels of PICI1 in NIL-*Pigm* (left panel) and NIPB (right panel) plants after inoculation with *M. oryzae* at the indicated time points. Actin was detected as a loading control. The protein abundance was quantified using ImageJ and indicated under lanes. **s**, RNA expression of *PICI1* was not significantly affected in late stage by blast infection (TH12 and TM21) in NIL-*Pigm*. For **d**, **e**, **f**, **k**, **l**, **s**, data are mean ± s.d. ($n = 3$, biologically independent samples). For **h**, **i**, **j**, **o**, **p**, data were analysed by two-tailed Student's *t*-test. Lesion lengths or areas (mean ± s.d.; n = numbers of biologically independent samples in the graphs), fungal growth (mean ± s.d.; $n = 3$, biologically independent samples). Lowercase letters indicate statistical significance ($P < 0.05$) (**a**, **m**, **q**). Asterisks indicate significant differences ($^*P < 0.05$, $^{**}P < 0.01$) (**b**, **c**, **g**–**j**, **o**, **p**). Exact *P* values are provided in Supplementary Table 4 (**a**–**c**, **g**-**j**, **m**, **o**–**q**). The rice *ACTIN1* served as an internal control (**d**–**g**, **k**, **l**, **s**). Scale bars, 1 cm (**h**–**j**, **o**–**q**). Experiments were repeated twice (**d**–**g**) three times with similar results (**a**–**c**, **h**–**j**, **k**–**m**, **o**-**q**, **r**, **s**).

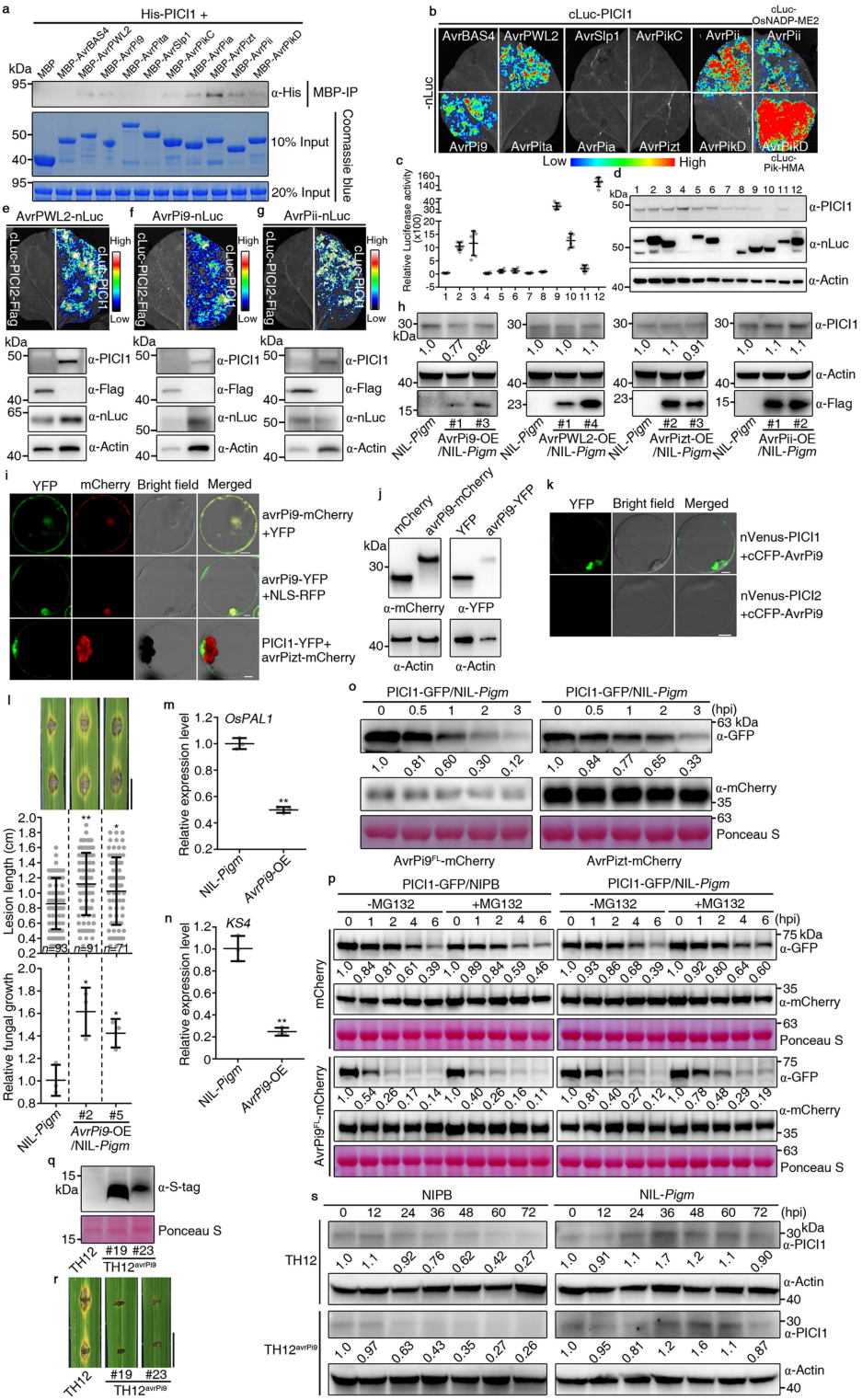

Extended Data Fig. 8 | See next page for caption.

Extended Data Fig. 8 | PigmR protects PICI1 from AvrPi9-mediated degradation. a, His-PICI1 could be pulled down by seven effectors (AvrPWL2, AvrPi9, AvrPikC, AvrPia, AvrPizt, AvrPii and AvrPikD fused with MBP) in vitro. MBP alone served as a negative control. **b**, SLC verification of the interactions between PICI1 and the three blast fungal effectors, AvrPWL2, AvrPi9 and AvrPii in *N. benthamiana*. Note that AvrPikD/Pik-HMA and AvrPii/OsNADP-ME2 served as positive controls. **c**, Relative luciferase activity of protein-protein interactions was measured. Data are mean ± s.d. ($n = 6$, biologically independent samples). **d**, Western blot confirming protein expression in *N. benthamiana*. Note that 1-12 represented PICI1/AvrBAS4, PICI1/AvrPWL2, PICI1/AvrPi9, PICI1/AvrPita, PICI1/AvrSlp1, PICI1/AvrPikC, PICI1/AvrPia, PICI1/AvrPizt, PICI1/AvrPii, OsNADP-ME2/PICI1, PICI1/AvrPikD and Pik-HMA/AvrPikD, respectively. **e**–**g**, SLC assays showed that PICI1, but not PICI2, specifically interacted with AvrPWL2 (**e**), AvrPi9 (**f**) and AvrPii (**g**) in *N. benthamiana*. Fluorescence signal intensity is indicated. Protein expression in *N. benthamiana* was detected by western blot (**e**-**g**, down panel). **h**, Protein levels of endogenous PICI1 in AvrPi9-Flag (AvrPi9-OE), AvrPWL2-Flag (AvrPWL2-OE), AvrPizt-Flag (AvrPizt-OE), and AvrPii-Flag (AvrPii-OE), compared with NIL-*Pigm*. The protein abundance was quantified and indicated under lanes. **i**, Subcellular localization of AvrPi9 and co-localization of PICI1-YFP/AvrPizt-mCherry in rice protoplasts. **j**, Western blot analysis confirming expression of AvrPi9-mCherry or AvrPi9-YFP without free mCherry or YFP in rice protoplasts. **k**, BiFC confirms the PICI1/AvrPi9 interaction in rice protoplasts. PICI2 served as a negative control. **l**, Basal blast resistance of WT and *AvrPi9*-OE lines, 5 dpi with TM21. Scale bars, 1 cm. Data were analysed by two-tailed Student's *t*-test. Lesion lengths (mean ± s.d.; n = numbers of biologically independent samples in the graphs), fungal growth (mean ± s.d.; $n = 3$, biologically independent samples). **m**, **n**, Induction of the PTI-related defence genes Os*PAL1* (**m**) and *KS4* (**n**) at 1 h after chitin incubation in WT and *AvrPi9*-OE. Two-tailed Student's *t*-test (mean ± s.d.; $n = 3$, biologically independent samples). The rice *ACTIN1* served as an internal control. **o**, Cell-free degradation shows AvrPi9^{FL}-mediated PICI1-GFP degradation. Protein extracts were prepared from two-week-old PICI1-GFP/NIL-*Pigm* seedlings and then incubated with AvrPi9^{FL}-mCherry or AvrPizt-mCherry expressed in *N. benthamiana*. **p**, Cell-free degradation shows the AvrPi9^{FL}-mediated PICI1-GFP degradation in NIPB (left panel) and NIL-*Pigm* (right panel) with or without MG132. Protein extracts were prepared from PICI1-GFP/NIPB and PICI1-GFP/NIL-*Pigm* seedlings and then incubated with mCherry (upper panels) or AvrPi9-mCherry (lower panels) expressed in *N. benthamiana*. FL, full length (**o**, **p**), and we used the Avrs without signal peptide to make the constructs in the experiments unless otherwise indicated. **q**, Immunodetection of two independent transformants of TH12^{AvrPi9} using an anti-S-tag antibody, with its parent TH12 as a negative control. Full length of AvrPi9 tagged by S-tag was transformed into TH12 by *Agrobacterium*-mediated transformation. **r**, Pathogenicity test of the transformants with TH12 as a virulent control. **s**, Protein levels of PICI1 in NIPB (left panel) and NIL-*Pigm* (right panel) after inoculation with TH12 (upper panel) or TH12^{AvrPi9} (lower panel). The protein abundance was quantified using ImageJ and indicated under lanes. Ponceau S staining (**o**–**q**) or Actin (**d**–**h**, **j**, **s**) served as loading control. Scale bars, 5 μm (**i**, **k**). Asterisks represent significant difference (*$P < 0.05$, **$P < 0.01$) (**l**-**n**). Exact *P* values are provided in Supplementary Table 4 (**l**–**n**). Experiments were repeated twice (**a**, **d**, **h**, **j**, **q**, **s**) or three times (**b**, **c**, **e**–**g**, **i**, **k**-**p**, **r**) with similar results.

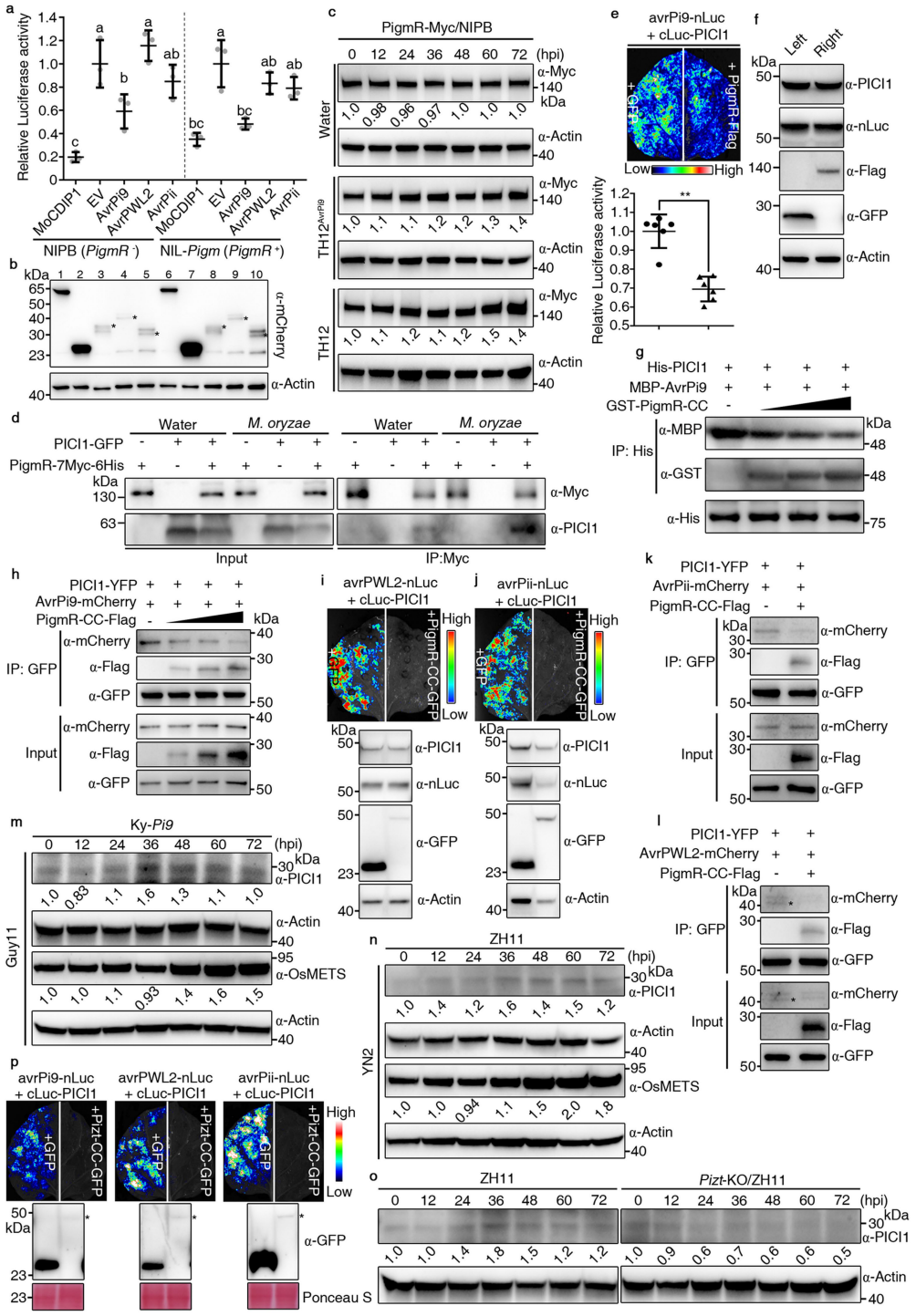

Extended Data Fig. 9 | See next page for caption.

Extended Data Fig. 9 | PigmR and Pizt protect PICI1 from Avrs binding in a competitive manner. a, PICI1-interacting effectors including AvrPi9, AvrPWL2 and AvrPii can not activate PigmR-mediated cell death. Relative luciferase activity was measured after transformation with different effectors in NIPB or NIL-*Pigm*. Empty vector (EV) and MoCDIP1 were used as negative and positive control, respectively. One-way ANOVA with Tukey's test (mean ± s.d.; $n = 3$, biologically independent experiments). Different letters indicate significant difference at $P < 0.05$. **b**, Western blot analysis confirming expression of proteins in rice protoplasts. Note that 1-5 and 6-10 represented MoCDIP1, EV, AvrPi9, AvrPWL2 and AvrPii in NIPB and NIL-*Pigm*, respectively. The asterisks indicate the target proteins. **c**, Increased protein accumulation of PigmR in PigmR-7Myc-His/NIPB after inoculation with TH12 or TH12^{AvrPi9} with water as a control at the indicated time points. **d**, PICI1-PigmR interaction is enhanced by *M. oryzae* infection. Proteins were prepared from transgenic plants PICI1-GFP/NIL-*Pigm* and PigmR-7Myc-His/NIPB after inoculation with TH12 or water as a control (36 hpi). **e**, A SLC assay shows that the PigmR disrupts PICI1-AvrPi9 interaction in *N. benthamiana*. Relative luciferase activity of protein-protein interactions was measured (lower panel). Two-tailed Student's *t*-test (mean ± s.d.; $n = 6$, biologically independent samples). The asterisk represents significant difference (**$P < 0.01$). **f**, Western blot confirming protein expression in *N. benthamiana*. Note that left and right represent PICI1/AvrPi9/GFP and PICI1/AvrPi9/PigmR combination, respectively. **g**, PigmR-CC outcompetes AvrPi9 for PICI1 binding in vitro. **h**, PigmR-CC outcompetes AvrPi9 for PICI1 binding in rice protoplasts. **i**, **j**, SLC assays show that the PigmR-CC also disrupts PICI1/AvrPWL2 (**i**) and PICI1/AvrPii (**j**) interactions in *N. benthamiana*. Protein expression in *N. benthamiana* was detected by western blot (lower panel) (**i**, **j**). **k**, **l**, PigmR-CC outcompetes AvrPii (**k**) or AvrPWL2 (**l**) for PICI1 binding in rice protoplasts. The asterisks indicate the target proteins (**l**). **m**, **n**, Protein accumulation of PICI1 and OsMETS in Ky-*Pi9* (**m**) and ZH11 (**n**) plants after inoculation with avirulent strain Guy11 (**m**) or YN2 (**n**) at the indicated time points. **o**, Protein accumulation of PICI1 in ZH11 and *Pizt*-KO/ZH11 plants after inoculation with blast strain CH131 (avirulent to Pizt) at the indicated time points. **p**, SLC assays show that the Pizt-CC also disrupts PICI1/AvrPi9 (left panel), PICI1/AvrPWL2 (middle panel) and PICI1/AvrPii (right panel) interactions in *N. benthamiana*. Protein expression in *N. benthamiana* was detected by western blot (lower panel). Actin (**b**, **c**, **f**, **i**, **j**, **m**–**o**) or Ponceau S staining (**p**) used as loading control. The protein abundance was quantified using ImageJ and indicated under lanes (**c**, **m**-**o**). Fluorescence signal intensity is indicated (**e**, **i**, **j**, **p**). Exact *P* values are provided in Supplementary Table 4 (**a**, **e**). Experiments were repeated twice (**b**, **d**, **f**, **g**, **h**, **k**-**p**) or three times (**a**, **c**, **e**, **i**, **j**) with similar results.

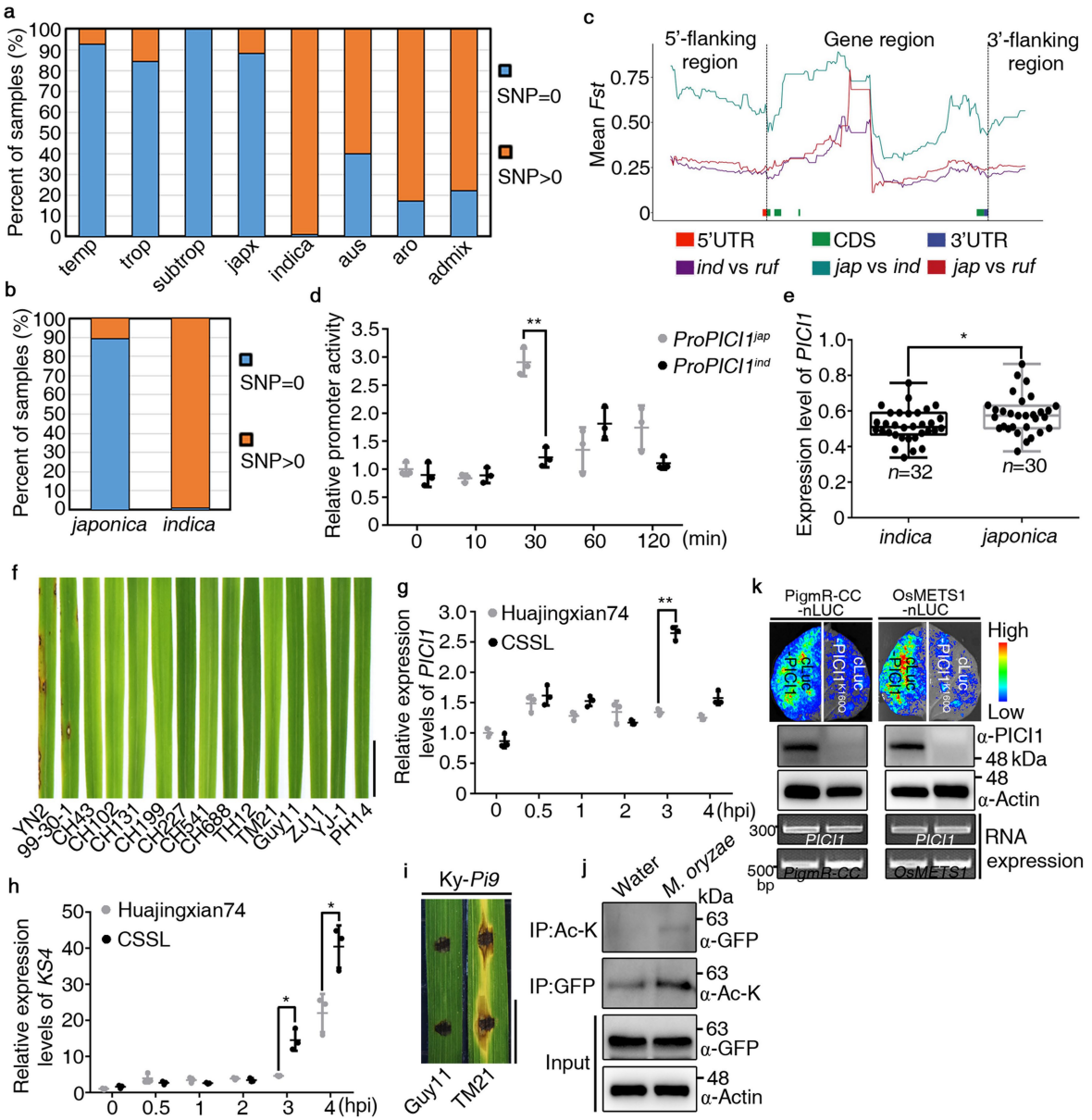

Extended Data Fig. 10 | *PICI1*^{jap} allele shows higher *PICI1* expression and increased basal defence, and acetylation of PICI1 promotes its degradation. a, Twenty-seven SNPs in the *PICI1* promoter distribute in different rice varieties based on the 3,000 Rice Genome database[33]. SNP = 0 indicates the same promoter sequence of *PICI1* with NIPB, which was used as the referee. SNP > 0 indicated at least one base change. **b**, Distribution of the 27 SNPs in *japonica* and *indica* rice based on the 3,000 Rice Genome Project database. **c**, F_{ST} of *PICI1* and flanking regions between different rice groups. **d**, Induction of *ProPICI1*^{ind}*-LUC* and *ProPICI1*^{jap}*-LUC* in rice protoplasts by chitin. LUC activity was measured by normalizing to REN signal. **e**, *japonica* rice varieties showed a general higher induction of *PICI1* than *indica* varieties by *M. oryzae* cocktail at 3 hpi. In box plots, the centre line represents the median, box edges delimit lower and upper quartiles and whiskers show the highest and lowest data points. Two-tailed Student's *t*-test (mean ± s.d.; *n* = numbers of biologically independent samples in the graphs). **f**, Pathotype test of different *M. oryzae* strains in two-week-old seedlings of Huajingxian74 using spraying inoculation, indicating YN2 and 99-30-1 virulent toward Huajingxian74. **g**, Induction of *PICI1* at indicated times by *M. oryzae* infection in Huajingxian74 and CSSL. **h**, Induction of the defence gene *KS4* after blast inoculation in Huajingxian74 and CSSL plants. **i**, Pathotype test of *M. oryzae* isolate and Guy11 (avirulent) and TM21 (virulent) toward *Pi9*-containing rice plant (Ky-*Pi9*) with punch inoculation. **j**, Increased acetylation of PICI1 after blast infection. The protein extracts from PICI1-GFP/NIL-*Pigm* plants challenged with *M. oryzae* (TM21) or water for 36 h were immunoprecipitated with Ac-K (Acetylated-lysine) or GFP antibody and analysed using anti-GFP or anti-Ac-K antibody, respectively. **k**, A SLC assay shows the reduced interaction of PICI1^{K160Q}/PigmR-CC and PICI1^{K160Q}/OsMETS1 in comparison with PICI1 in *N. benthamiana*. The protein and transcript levels of cLuc-PICI1 and cLuc-PICI1^{K160Q} were determined by immunoblot and semi-quantitative PCR. Actin was detected as a loading control (**j**, **k**). The rice *ACTIN1* served as an internal control (**e**, **g**, **h**). Two-tailed Student's *t*-test (mean ± s.d.; *n* = 3, biologically independent samples) (**d**, **g**, **h**). Asterisks indicate significant differences (*$P < 0.05$, **$P < 0.01$) (**d**, **e**, **g**, **h**). Exact *P* values are provided in Supplementary Table 4 (**d**, **e**, **g**, **h**). Scale bars, 1 cm (**f**, **i**). Experiments were repeated twice (**e**, **g**, **h**) or three times (**d**, **f**, **i**-**k**) with similar results.

nature research

Corresponding author(s): Zuhua He

Last updated by author(s): Sep 29, 2021

Reporting Summary

Nature Research wishes to improve the reproducibility of the work that we publish. This form provides structure for consistency and transparency in reporting. For further information on Nature Research policies, see our Editorial Policies and the Editorial Policy Checklist.

Statistics

For all statistical analyses, confirm that the following items are present in the figure legend, table legend, main text, or Methods section.

n/a	Confirmed	
☐	☒	The exact sample size (*n*) for each experimental group/condition, given as a discrete number and unit of measurement
☐	☒	A statement on whether measurements were taken from distinct samples or whether the same sample was measured repeatedly
☐	☒	The statistical test(s) used AND whether they are one- or two-sided *Only common tests should be described solely by name; describe more complex techniques in the Methods section.*
☒	☐	A description of all covariates tested
☐	☒	A description of any assumptions or corrections, such as tests of normality and adjustment for multiple comparisons
☐	☒	A full description of the statistical parameters including central tendency (e.g. means) or other basic estimates (e.g. regression coefficient) AND variation (e.g. standard deviation) or associated estimates of uncertainty (e.g. confidence intervals)
☐	☒	For null hypothesis testing, the test statistic (e.g. *F*, *t*, *r*) with confidence intervals, effect sizes, degrees of freedom and *P* value noted *Give P values as exact values whenever suitable.*
☒	☐	For Bayesian analysis, information on the choice of priors and Markov chain Monte Carlo settings
☒	☐	For hierarchical and complex designs, identification of the appropriate level for tests and full reporting of outcomes
☒	☐	Estimates of effect sizes (e.g. Cohen's *d*, Pearson's *r*), indicating how they were calculated

Our web collection on statistics for biologists contains articles on many of the points above.

Software and code

Policy information about availability of computer code

Data collection	The fluorescence signal was detected using a confocal microscope (Olympus Fluoview FV1000). Images from immuno blotting and luciferase were collected with Tanon MP (5500). Luminescence was monitored with a Glomax 20/20 luminometer (Promega) or Varioskan Flash multireader (Thermo Fisher Scientific, 6.0). Protein MS/MS was analyzed with Q ExactiveTM (Thermo Fisher Scientific).
Data analysis	Structure visualization: PYMOL molecular viewer (version 2.1) Image analysis: ImageJ (version 1.45) Statistical analysis: GraphPad Prism (version 6.01), Excel 2016 (Microsoft) Alignments: MegAlign (version 7.1.0) Proteomic analysis: Mascot (v 2.3.02 Matrix Science)

For manuscripts utilizing custom algorithms or software that are central to the research but not yet described in published literature, software must be made available to editors and reviewers. We strongly encourage code deposition in a community repository (e.g. GitHub). See the Nature Research guidelines for submitting code & software for further information.

Data

Policy information about availability of data

All manuscripts must include a data availability statement. This statement should provide the following information, where applicable:

- Accession codes, unique identifiers, or web links for publicly available datasets
- A list of figures that have associated raw data
- A description of any restrictions on data availability

All data are available within this Article and its Supplementary Information. Original gel blots are shown in Supplementary Fig. 1. Original data points in graphs are shown in Source Data files. Statistical analyses of this study are provided in Supplementary Table 4. The sequences of PICI1, OsMETS1 and OsMETS2 have been

deposited and made publicly available in the GenBank with accession code MT920667, MT920668 and MT920669, respectively. Protein structure models of PDB ID 2WP7 (https://www.rcsb.org/structure/2WP7) and PDB ID 1U1U (https://www.rcsb.org/structure/1U1U) were obtained from Protein Data Bank.

Field-specific reporting

Please select the one below that is the best fit for your research. If you are not sure, read the appropriate sections before making your selection.

☒ Life sciences ☐ Behavioural & social sciences ☐ Ecological, evolutionary & environmental sciences

For a reference copy of the document with all sections, see nature.com/documents/nr-reporting-summary-flat.pdf

Life sciences study design

All studies must disclose on these points even when the disclosure is negative.

Sample size	Sample size was determined based on experimental trials and previous publications on similar experiments. No statistical methods were used to predetermine sample size. Previous publications considered to determine sample size include: Gene expression analysis (doi: 10.1126/science.aai8898) Lesion length/area and fungal growth analysis (doi: 10.1126/science.aai8898; doi: 10.1016/j.molcel.2019.03.013.) ROS burst (doi: 10.1105/tpc.112.105429; doi: 10.1038/s41586-021-03316-6) Promoter activity (doi: 10.1016/j.molcel.2019.03.013) Agronomic traits (doi: 10.1126/science.aai8898) Cell death assay (doi.org/10.1094/MPMI-05-12-0117-R) Relative luciferase activity (doi: 10.1371/journal.ppat.1006878) Ethylene and methionine measurement (doi: 10.7554/eLife.27529)
Data exclusions	No data were excluded.
Replication	All experiments were successfully repeated at least two or three times, and the number of independent experiments or biological replicates is indicated in the figure legends.
Randomization	Plants were randomly assigned to the treatment and control groups with no formal randomization techniques.
Blinding	Investigators were not blinded to the allocation during experiments as it does not include clinical trials. The research materials are plants so the blind design is not applicable in the field. Researchers were not blinded to plant genotypes during experiments. Experiments were conducted by different authors, whenever possible.

Reporting for specific materials, systems and methods

We require information from authors about some types of materials, experimental systems and methods used in many studies. Here, indicate whether each material, system or method listed is relevant to your study. If you are not sure if a list item applies to your research, read the appropriate section before selecting a response.

Materials & experimental systems

n/a	Involved in the study
☐	☒ Antibodies
☒	☐ Eukaryotic cell lines
☒	☐ Palaeontology and archaeology
☒	☐ Animals and other organisms
☒	☐ Human research participants
☒	☐ Clinical data
☒	☐ Dual use research of concern

Methods

n/a	Involved in the study
☒	☐ ChIP-seq
☒	☐ Flow cytometry
☒	☐ MRI-based neuroimaging

Antibodies

Antibodies used	anti-Myc (MILLIPORE, Cat#05-724, 1:2000) anti-His (CWBIO, Cat#CW0286M, 1:1000) anti-MBP (CWBIO, Cat#CW0288M, 1:1000) anti-Ub (polyubiquitin) (Cell Signaling Technology, Cat#3936S, 1:1000) anti-K63 (K63-linkage specific polyubiquitin) (Cell Signaling Technology, Cat#5621S, 1:1000) anti-K48 (K48-linkage specific polyubiquitin) (Cell Signaling Technology, Cat#8081S, 1:1000) anti-Ac-K (Acetylated-Lysine (Ac-K-103)) (Cell Signaling Technology, Cat#9681S, 1:1000) anti-Actin (CMCTAG, Cat#AT0004, 1:2000) anti-mCherry (Abcam, Cat#ab125096, 1:1000) anti-Flag (Sigma, Cat#F1804, 1:2000)

anti-GFP (Abcam, Cat#ab290, 1:2000)
anti-S tag (Abcam, Cat#ab183674, 1:1000)
anti-GAL4-BD (Abcam, Cat#ab135397, 1:1000)
anti-GAL4-AD (Sigma-Aldrich, Cat#G9293, 1:1000)
anti-nLuc (Firefly luciferase) (Abcam, Cat#ab185924, 1:1000)
anti-PICI1 (custom-developed by ABclonal® Technology, China, 1:1000)
anti-OsMETS (custom-developed by ABclonal® Technology, China, 1:1000)
Goat anti-Rabbit IgG Secondary Antibody, HRP conjugate (Thermo Fisher, Cat#31460, 1:10000)
Goat anti-mouse IgG Secondary Antibody, HRP conjugate (BIO-RAD, Cat#170-6516, 1:10000)

Validation

Validation statements and experiments can be obtained from the following websites and publications:
anti-Myc (https://www.merckmillipore.com/CN/zh/product/Anti-Myc-Tag-Antibody-clone-4A6,MM_NF-05-724)
anti-His (https://www.cwbio.com/goods/index/id/10177)
anti-MBP (DOI: 10.1126/science.aai8898)
anti-Ub (https://www.cellsignal.com/products/primary-antibodies/ubiquitin-p4d1-mouse-mab/3936?site-search-type=Products&N=4294956287&Ntt=3936S&fromPage=plp&_requestid=318079)
anti-K63 (https://www.cellsignal.com/products/primary-antibodies/k63-linkage-specific-polyubiquitin-d7a11-rabbit-mab/5621?site-search-type=Products&N=4294956287&Ntt=5621S&fromPage=plp&_requestid=318228)
anti-K48 (https://www.cellsignal.com/products/primary-antibodies/k48-linkage-specific-polyubiquitin-d9d5-rabbit-mab/8081?site-search-type=Products&N=4294956287&Ntt=8081S&fromPage=plp&_requestid=318306)
anti-Ac-K (https://www.cellsignal.com/products/primary-antibodies/acetylated-lysine-mouse-mab-ac-k-103/9681?site-search-type=Products&N=4294956287&Ntt=9681S&fromPage=plp&_requestid=318414)
anti-Actin (doi: 10.1038/s41422-019-0145-8)
anti-mCherry (https://www.abcam.cn/mcherry-antibody-1c51-ab125096.html)
anti-Flag (https://www.sigmaaldrich.cn/CN/zh/product/sigma/f1804?context=product)
anti-GFP (https://www.abcam.cn/gfp-antibody-ab290.html)
anti-S tag (https://www.abcam.cn/s-tag-antibody-ab183674.html)
anti-GAL4-BD (https://www.abcam.cn/gal4-antibody-15-6e10a7-ab135397.html)
anti-GAL4-AD (https://www.sigmaaldrich.cn/CN/zh/product/sigma/g9293?context=product)
anti-nLuc (https://www.abcam.cn/firefly-luciferase-antibody-epr17790-ab185924.html)
anti-PICI1 (custom-developed by ABclonal® Technology, China, 1:1000; Extended data Fig. 2b, p in this study)
anti-OsMETS (custom-developed by ABclonal® Technology, China, 1:1000; Extended data Fig. 5o, q in this study)
Goat anti-Rabbit IgG Secondary Antibody (https://www.thermofisher.cn/cn/zh/antibody/product/Goat-anti-Rabbit-IgG-H-L-Secondary-Antibody-Polyclonal/31460)
Goat anti-mouse IgG Secondary Antibody (https://www.bio-rad.com/zh-cn/sku/1706516-goat-anti-mouse-igg-h-l-hrp-conjugate?ID=1706516)